
Article:
Cheung, K.Y. orcid.org/0000-0002-1098-4926, Jesuthasan, S.J., Baxendale, S. orcid.org/0000-0002-6760-9457 et al. (4 more authors) (2021) Olfactory rod cells : a rare cell type in the larval zebrafish olfactory epithelium with a large actin-rich apical projection. Frontiers in Physiology, 12 (1). 626080.

https://doi.org/10.3389/fphys.2021.626080

---

frontiers in Physiology

ORIGINAL RESEARCH
published: 26 February 2021
doi: 10.3389/fphys.2021.626080

Olfactory Rod Cells: A Rare Cell Type in the Larval Zebrafish Olfactory Epithelium With a Large Actin-Rich Apical Projection

King Yee Cheung[1†], Suresh J. Jesuthasan[2,3†], Sarah Baxendale[1†], Nicholas J. van Hateren[1†], Mar Marzo[1†], Christopher J. Hill[1†] and Tanya T. Whitfield[1*†]*

[1] Department of Biomedical Science, Bateson Centre and Neuroscience Institute, University of Sheffield, Sheffield, United Kingdom, [2] Lee Kong Chian School of Medicine, Nanyang Technological University, Singapore, Singapore, [3] Institute of Molecular and Cell Biology, Singapore, Singapore

We report the presence of a rare cell type, the olfactory rod cell, in the developing zebrafish olfactory epithelium. These cells each bear a single actin-rich rod-like apical projection extending 5–10 μm from the epithelial surface. Live imaging with a ubiquitous Lifeact-RFP label indicates that the olfactory rods can oscillate. Olfactory rods arise within a few hours of the olfactory pit opening, increase in numbers and size during larval stages, and can develop in the absence of olfactory cilia. Olfactory rod cells differ in morphology from the known classes of olfactory sensory neuron, but express reporters driven by neuronal promoters. A sub-population of olfactory rod cells expresses a Lifeact-mRFPruby transgene driven by the *sox10* promoter. Mosaic expression of this transgene reveals that olfactory rod cells have rounded cell bodies located apically in the olfactory epithelium and have no detectable axon. We offer speculation on the possible function of these cells in the Discussion.

Keywords: olfactory rod cell, olfactory placode, olfactory epithelium, actin, actin-rich projection, Lifeact, zebrafish

OPEN ACCESS

Edited by:
Patrick Blader, FR3743 Centre de Biologie Intégrative (CBI), France

Reviewed by:
Erika Calvo-Ochoa, Hope College, United States
Thomas Schilling, University of California, Irvine, United States

***Correspondence:**
Tanya T. Whitfield
t.whitfield@sheffield.ac.uk
Suresh J. Jesuthasan
sureshjj@imcb.a-star.edu.sg;
sureshj@ntu.edu.sg

†ORCID:
King Yee Cheung
orcid.org/0000-0002-1098-4926
Suresh J. Jesuthasan
orcid.org/0000-0002-5733-6555
Sarah Baxendale
orcid.org/0000-0002-6760-9457
Nicholas J. van Hateren
orcid.org/0000-0002-0011-9947
Mar Marzo
orcid.org/0000-0003-1591-0309
Christopher J. Hill
orcid.org/0000-0002-6914-4411
Tanya T. Whitfield
orcid.org/0000-0003-1575-1504

Specialty section:
This article was submitted to Craniofacial Biology and Dental Research, a section of the journal Frontiers in Physiology

Received: *04 November 2020*
Accepted: *25 January 2021*
Published: *26 February 2021*

Citation:
Cheung KY, Jesuthasan SJ, Baxendale S, van Hateren NJ, Marzo M, Hill CJ and Whitfield TT (2021) Olfactory Rod Cells: A Rare Cell Type in the Larval Zebrafish Olfactory Epithelium With a Large Actin-Rich Apical Projection. Front. Physiol. 12:626080. doi: 10.3389/fphys.2021.626080

INTRODUCTION

The vertebrate olfactory epithelium (OE) is a multimodal sensor. The functions of this epithelium, which derives from paired cranial neurogenic placodes (Whitlock and Westerfield, 2000), are mediated by a diverse set of cells. Two broad classes of sensory receptor—ciliated and microvillous—have been identified in the OE on the basis of morphology, receptor expression, and projection pattern (reviewed in Elsaesser and Paysan, 2007). Olfactory sensory neurons (OSNs), which express G-protein-coupled odorant receptors (ORs) and give rise to the sense of smell, are bipolar neurons that extend a dendrite to the apical surface of the OE and an axon to the olfactory bulb (OB; reviewed in Axel, 1995). Other sensory cells, some of which have no detectable axon, are also present. In mammals, these include microvillous cells that express TrpM channels and other taste components (Hansen and Finger, 2008; Lin et al., 2008; Genovese and Tizzano, 2018); such solitary chemosensory cells (SCCs) also exist in alligators (Hansen, 2007). A subset of OSNs can act as mechanosensors (Grosmaitre et al., 2007; Brinkmann and Schild, 2016; Iwata et al., 2017). Thus, the wide range of cell types in the OE allows for the detection of mechanical and other chemical stimuli in addition to sensing odours.

This variety of receptors is seen not only in terrestrial (air-breathing) animals, but also in aquatic vertebrates. In zebrafish, five classes of OSN have been identified. Each occupies a stereotyped

position within the pseudostratified OE, with the dendrite bearing a distinct and characteristic specialisation projecting into the environment (Hansen and Zeiske, 1998; Hansen and Zielinski, 2005; Sato et al., 2005; reviewed in Maier et al., 2014). Ciliated neurons, which express olfactory marker protein (OMP) and OR genes, have a cell body that lies deep within the OE, an axon that projects to dorsal and medial regions of the OB, and a slender dendrite extending to the surface of the olfactory pit. Here, the dendritic knob bears a cluster of primary cilia that project into the olfactory cavity (Hansen and Zeiske, 1998; Hansen and Zielinski, 2005; Sato et al., 2005). Microvillous OSNs, characterised by the expression of TrpC2 and vomeronasal (VR)-type pheromone receptors, have cell bodies that lie in the intermediary layer of the OE, an axon that projects to the lateral part of the OB, and a dendrite bearing a tuft of short, actin-rich microvilli (Hansen and Zeiske, 1998; Hansen and Zielinski, 2005; Sato et al., 2005). Crypt neurons, less abundant than ciliated or microvillous OSNs, have rounded cell bodies that sit apically in the OE, with both cilia and microvilli extending from a crypt within the cell body (Hansen and Zeiske, 1998; Hansen and Zielinski, 2005; Parisi et al., 2014; Biechl et al., 2016; Bettini et al., 2017; Sepahi et al., 2019). Kappe neurons lie in the superficial layers of the adult zebrafish OE and are named for their apical actin-rich cap, presumed to be microvilli (Ahuja et al., 2014). Pear-shaped neurons are also positioned superficially in the adult OE and have short apical dendrites, but express some markers in common with ciliated neurons (Wakisaka et al., 2017). Aside from these OSNs, it is not known what other sensory cell types exist.

The OE is directly exposed to the environment, and is thus continually subject to damage and infection. Numerous mechanisms enable efficient sampling of stimuli while maintaining tissue integrity and defence. These functions are provided by non-sensory cells in the OE, which include basal (stem) cells that replenish the OSNs, sustentacular (support) cells, and goblet cells, which produce mucus containing anti-microbial peptides (Hansen and Zeiske, 1993, 1998; Byrd and Brunjes, 1995; Demirler et al., 2019; reviewed in Olivares and Schmachtenberg, 2019). Multiciliated cells, located around the rim of the olfactory pit in fish, each bear multiple long motile cilia. These have a characteristic 9+2 axoneme and beat at around 24 Hz, resulting in an asymmetric flow that draws water and odorants into the olfactory cavity and flushes them out again (Reiten et al., 2017). Additional cell types with critical functions, such as immune cells, also populate the OE (Sepahi et al., 2019; Kraus et al., 2020).

We report here the existence of a rare cell type, the olfactory rod cell, in the OE of larval zebrafish. Olfactory rod cells are characterised by a single actin-rich apical projection, and were initially observed in whole-mount phalloidin stains, which we use routinely to visualise the actin-rich stereociliary bundles on sensory hair cells of the inner ear and lateral line. It was unclear what these olfactory cells were, as they did not resemble previously described OSNs. The morphology of the olfactory rod matches descriptions of similar structures in the OE of several other fish species (Bannister, 1965; Schulte, 1972; Breipohl et al., 1973; Ichikawa and Ueda, 1977; Yamamoto and Ueda, 1978; Rhein et al., 1981; Hernádi, 1993; Datta and Bandopadhyay, 1997), many of which were previously dismissed either as senescent forms of OSNs or as fixation artefacts (Muller and Marc, 1984; Moran et al., 1992). Using a variety of transgenic lines and imaging techniques, including live imaging, we show that zebrafish olfactory rod cells are present in living fish and can be detected from early stages of larval development.

MATERIALS AND METHODS

Zebrafish Husbandry

Zebrafish strains used in this study were wild type (AB strain—ZFIN), *ift88*^{tz288b} (Tsujikawa and Malicki, 2004), *sox10*^{m618} (Dutton et al., 2001), *Tg(actb2:Lifeact-RFP)*^{e115} (Behrndt et al., 2012), *Tg*(*actb2:Lifeact-GFP)*^{e114} (Behrndt et al., 2012), *Tg(Xla.Tubb:jGCaMP7f)*^{sq214} (Chia et al., 2019), *Tg(elavl3:GCaMP6f)*^{jf1} (Dunn et al., 2016), *Tg(elavl3:H2B-GCaMP6s)*^{jf5} (Dunn et al., 2016), *Tg(pou4f3:GAP-GFP)*^{s356t} (Xiao et al., 2005) and *Tg(sox10:Lifeact-mRFPruby)*^{sh630} (this study). Homozygous *sox10*$^{-/-}$ mutant larvae were identified by their lack of body pigmentation at 5 days post-fertilisation (dpf). Adult zebrafish were kept in a 10 h dark/14 h light cycle at 28.5°C and spawned by pair-mating or marbling (Aleström et al., 2019). Eggs were collected and staged according to standard protocols (Kimmel et al., 1995; Nüsslein-Volhard and Dahm, 2002), and raised in E3 medium (5 mM NaCl, 0.17 mM KCl, 0.33 mM $CaCl_2$, 0.33 mM $MgSO_4$, with 0.0001% methylene blue at early stages) at 28.5°C. For controlling the developmental rate to obtain embryos at stages 34–46 h post-fertilisation (hpf), embryos were incubated at 25°C or 34°C in accordance with Kimmel's formula, $_{H_T=h\div(0.055T-0.57)}$ (Kimmel et al., 1995). For live imaging, zebrafish were anaesthetised with 0.5 mM tricaine mesylate in E3.

Generation of the *Tg(sox10:Lifeact-mRFPruby)* Transgenic Line

The *-4725sox10:Lifeact-mRFPruby* construct was generated using the Gateway Tol2 kit (Kawakami, 2007; Kwan et al., 2007). The p5E *-4725sox10* promoter (Dutton et al., 2008; Rodrigues et al., 2012), pME-*Lifeact-mRFPruby* (Riedl et al., 2008), and p3E polyA sequences were cloned into pDestTol2pA3 through an LR Clonase reaction. The 12.1 kb final plasmid was sequenced and injected into the AB strain. Injected embryos were grown to adulthood and crossed to AB. Transgenic progeny from one founder male were selected based on mRFPruby expression in the inner ear and grown to adulthood to generate a stable line. Embryos with bright fluorescence, presumed to be homozygous for the transgene, were chosen for imaging.

Immunohistochemistry and Phalloidin Staining

Zebrafish embryos and larvae were fixed in 4% paraformaldehyde (PFA) in phosphate-buffered saline (PBS) for 2 h at room temperature or overnight at 4°C. Zebrafish were washed three or

more times with PBS, and permeabilised by incubation in PBS-Triton X-100 (0.2% Triton for 36–48 hpf embryos, 1% Triton for later stages) for several hours at 4°C until staining.

To visualise F-actin, zebrafish were stained with either Alexa Fluor 488 phalloidin (Cell Signaling Technology; 1:150), Alexa Fluor 568 (Invitrogen ThermoFisher; 1:50), or Alexa Fluor 647 phalloidin (Invitrogen ThermoFisher; 1:50) in PBS overnight at 4°C. After staining, zebrafish were washed four times in PBS over two or more hours before imaging.

For antibody staining, after fixing and washing, zebrafish were washed a further three times in PBS-0.2% Triton and incubated in blocking solution (10% sheep serum in PBS-0.2% Triton) for 60 min at room temperature. The primary antibody was mouse IgG1 anti-acetylated α-tubulin antibody (Sigma-Aldrich; 1:100). Staining was carried out in blocking solution containing 1% dimethyl sulfoxide (DMSO; Sigma-Aldrich) overnight at 4°C. Zebrafish were washed three times in PBS-0.2% Triton, and a further four times over two or more hours. The secondary antibody was Alexa 647-conjugated goat anti-mouse IgG1 (Invitrogen ThermoFisher; 1:200). For double stains with phalloidin, Alexa Fluor 488 phalloidin (1:150) and DMSO (1%) were added together with the secondary antibody in blocking solution overnight at 4°C. Zebrafish were then washed four times in PBS-0.2% Triton and stored at 4°C until imaging. Controls with no primary antibody yielded no staining (not shown).

Neomycin Treatment

For neomycin treatment, a concentration of 500 μM was chosen, as it was an effective concentration used by Harris et al. (2003) for minimum lateral line hair cell survival, as measured by DASPEI staining. A 5 mM solution was made by adding neomycin trisulfate salt hydrate (Sigma-Aldrich) to MilliQ water and used at a 1:10 dilution in E3 fish medium. *Tg(pou4f3:GFP)* transgenic zebrafish were treated for 60 min at 28.5°C. An equivalent volume of MilliQ water in E3 was used for the control group. Zebrafish were washed three times in fresh E3 and left at 28.5°C for 2 h. GFP signal was screened using widefield fluorescence microscopy to analyse hair cell damage. Zebrafish were fixed and stained with Alexa Fluor 647 phalloidin as above.

Fluorescence Imaging

For confocal imaging, fixed zebrafish embryos and larvae were mounted in 1.5% low melting point (LMP) agarose in PBS, and live zebrafish were mounted in 1.5% LMP agarose in E3 in WillCo glass-bottomed dishes (mounted in frontal view for 36–48 hpf, dorsal view for later stages). Zebrafish were imaged on a Zeiss LSM880 Airyscan confocal microscope equipped with a Plan-Apochromat 20 × /0.8 M27 air objective, LD LCI Plan-Apochromat 40 × /1.2 Imm Korr DIC M27 water immersion objective, or Plan-Apochromat 63 × /1.4 oil DIC M27 objective. Images were acquired in Airyscan SR mode, Airyscan Fast scan mode with SR sampling, or Airyscan Fast scan mode with Opt sampling. Zebrafish were also imaged on a Zeiss LSM 800 attached to an upright microscope with a W Plan-Apochromat 40 × /1.0 DIC M27 or 63 × /1.0 M27 water dipping objective. The laser lines used were 488, 561, and 633 nm. Widefield imaging was performed on a Zeiss Axio Zoom.V16 fluorescence stereo zoom microscope equipped with a Zeiss 60N-C 1" 1.0 × C-mount and AxioCam MRm camera. For light-sheet imaging, live zebrafish larvae were mounted in 0.9% LMP agarose in E3 and imaged on a Zeiss Z1 Light-sheet microscope, with 4% tricaine in E3 in the sample chamber. Imaging was performed with a W Plan-Apochromat 20 × objective using brightfield illumination and the 561 nm laser line.

Scanning Electron Microscopy

For scanning electron microscopy, *ift88* homozygous mutant and phenotypically wild-type sibling larvae at 4 dpf were fixed overnight in 2.5% glutaraldehyde/0.1M sodium cacodylate buffer. Samples were washed in buffer, post-fixed in 2% aqueous osmium tetroxide for 1 h, washed in buffer again and then dehydrated through a graded ethanol series (50, 75, 95, 100%) before being dried in a mixture of 50% hexamethyldisilazane (HMDS) in 100% ethanol. Final drying was in 100% HMDS. After removal of the final HMDS wash, samples were left to dry in a fume hood overnight. Samples were mounted onto a pin stub using a Leit-C sticky tab and Leit-C mounting putty, gold-coated using an Edwards S150B sputter coater, and examined in a Tescan Vega3 LMU Scanning Electron Microscope at an operating voltage of 15 kV and imaged using a secondary electron detector.

Image Processing, Quantification, and Statistical Analyses

Zeiss LSM880 Airyscan confocal images were subjected to Airyscan processing on Zen Black 2.3 software (Zeiss) using "Auto" Airyscan processing parameters. Further processing was performed on Fiji (Schindelin et al., 2012). 3D rendering was performed using the 3D Viewer plugin (Schmid et al., 2010) on Fiji. Olfactory rod projection lengths were measured in 3D from confocal images using Fiji, and calculated in Microsoft Excel using the PyT method (based on the Pythagorean theorem) from Dummer et al. (2016). All quantifications were exported into GraphPad Prism 8, which was then used for performing statistical analyses and making graphs.

Statistical analyses were carried out in GraphPad Prism 8. Datasets were considered normally distributed if they passed at least one of four normality tests (Anderson-Darling, D'Agostino & Pearson, Shapiro-Wilk, and Kolmogorov-Smirnov tests). Statistical tests used are stated in the figure legends. Bars on graphs indicate mean ± standard error of the mean (S.E.M.), unless stated otherwise. *P* values are indicated as follows: $P > 0.05$ (not significant, ns), $P < 0.05$ (*), $P < 0.01$ (**), $P < 0.001$ (***), $P < 0.0001$ (****).

For mapping spatial distributions of olfactory rod cells within the olfactory pit, 2D maximum intensity projection images were imported into the Desmos Graphing Calculator (desmos.com). The positions and sizes of the images were adjusted to align the rims of olfactory pits with an ellipse to fit the shape of the rim, defined by $\frac{(x-35)^2}{5}+\frac{(y-33)^2}{10}=7.6^2$. The positions of the base of each olfactory rod, relative to the ellipse, were plotted as coordinates onto the graph. The resulting graphs were exported as .png image files.

Figures were prepared using Adobe Photoshop and Affinity Designer.

RESULTS

Actin-Rich Rod-Like Apical Projections, Distinct From OSN Microvilli and Cilia, Are Present in the Olfactory Epithelium of Larval and Juvenile Zebrafish

Staining of the wild-type larval and juvenile zebrafish OE with fluorescently conjugated phalloidin, which binds to F-actin, reveals the presence of several actin-rich rod-like projections ("olfactory rods") in each olfactory pit (**Figures 1A–B′**). These projections differ in number, distribution, size and morphology from any of the described apical projections of zebrafish OSNs. The projections extend from below the apical surface of the OE and project about 5–10 μm above it, tapering to a point. This is an order of magnitude longer than OSN microvilli, which are typically 0.5–0.8 μm in length (Hansen and Zeiske, 1998). Olfactory rods are shorter than the surrounding phalloidin-negative olfactory cilia (**Figures 1C–D′**), and do not label with an anti-acetylated α-tubulin antibody (**Figures 1C–C‴**). Olfactory rods are not evenly distributed across the OE, but are mostly clustered posterolaterally in each olfactory pit, although there is variation between individuals (**Figure 1E**). At low magnification, the olfactory rods appear similar to the actin-rich stereociliary bundle of mechanosensory hair cells of the inner ear and lateral line. However, higher magnification images reveal that

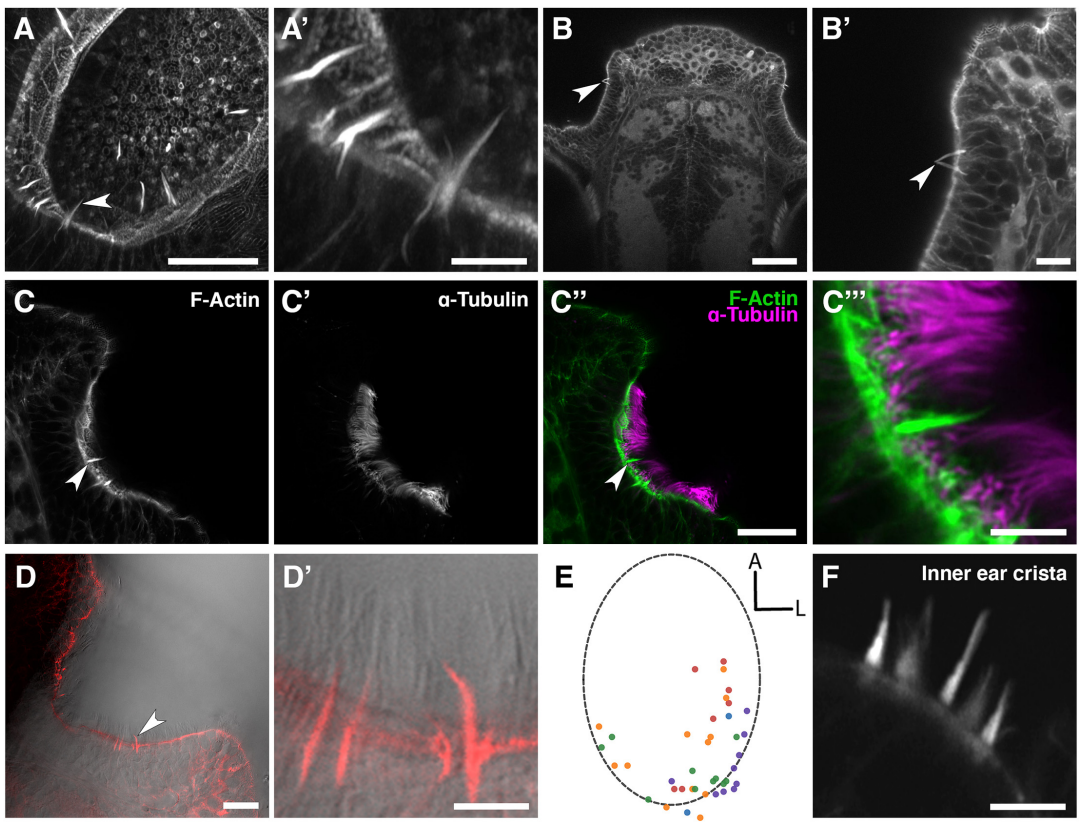

FIGURE 1 | Phalloidin staining reveals the presence of actin-rich rod-like projections, distinct from OSN microvilli and cilia, in the zebrafish larval and juvenile olfactory epithelium. **(A)** Maximum intensity projection of an Airyscan confocal image of phalloidin stain in an olfactory pit of a 5 dpf wild-type larva; anterior to the top right, lateral to the bottom right. Arrowhead marks one example olfactory rod. Scale bar = 20 μm. **(A′)** Enlargement of olfactory rods in panel **(A)**. Scale bar = 5 μm. **(B)** Dorsal view low power image of phalloidin stain in the head of an 18 dpf (5 mm) wild-type juvenile zebrafish; anterior to the top. Arrowhead marks the position of two olfactory rods in an olfactory pit. Scale bar = 50 μm. **(B′)** Enlargement of OE in panel **(B)**. Arrowhead marks two olfactory rods. Scale bar = 10 μm. **(C–C″)** Airyscan confocal image of Alexa-phalloidin signal **(C)**, acetylated α-tubulin immunohistochemistry signal **(C′)**, and merged signals **(C″)** in an olfactory pit of a 4 dpf wild-type larva; anterior to the top, lateral to the right. Arrowhead marks one example olfactory rod. Scale bar = 20 μm. **(C‴)** Enlargement of olfactory rod in panel **(C″)**. Scale bar = 5 μm. **(D)** Differential interference contrast (DIC) image and phalloidin stain (red) in an olfactory pit of a 5 dpf wild-type larva; anterior to the top, lateral to the right. Arrowhead marks one example olfactory rod. Scale bar = 20 μm. **(D′)** Enlargement of olfactory rods in panel **(D)**. Surrounding olfactory cilia are visible and unlabelled by Alexa-phalloidin. Scale bar = 5 μm. **(E)** A map of the positions of olfactory rod cell projection bases in olfactory pits of 4 dpf wild-type larvae (*N* of olfactory pits = 5), based on 2D maximum intensity projections of confocal images of phalloidin stains; anterior "A" to the top, lateral "L" to the right. One dot represents one olfactory rod. Different coloured dots represent olfactory rods from different larvae. **(F)** Airyscan confocal image of phalloidin stain in an inner ear crista of a 5 dpf wild-type larva. Hair cell stereocilia are labelled with Alexa-phalloidin, and are arranged in a stepped array. In the stereociliary bundle on the extreme left, four different stereociliary lengths are visible [compare with panel **(A′)**]. Scale bar = 5 μm.

the olfactory rod is not oligovillous, but appears to be a single structure (**Figures 1B′,C‴,D′**). This contrasts with the stepped array of multiple stereocilia present on the apical surface of mechanosensory hair cells (**Figure 1F**).

To characterise the timing of appearance and development of the olfactory rods during embryonic and larval stages, we stained fixed samples from 36 hpf, just after formation of the olfactory pits (Hansen and Zeiske, 1993), to 5 dpf. Occasional olfactory rods were present in olfactory pits at 36 hpf, but were only consistently present beyond 46 hpf (**Figures 2A,B**). Although the number of olfactory rods per pit varied at each stage, the average number increased over time. By 5 dpf, each pit contained 10.7 ± 2.9 (mean ± standard deviation, SD) olfactory rods (**Figure 2B**). After measuring the olfactory rods in 3D, we found an increase in projection length (from the base of the phalloidin-positive projection to the tip) from 36 hpf to 5 dpf, with the most significant increase occurring by 48 hpf, despite a relatively large range in length at each stage. At 5 dpf in fixed samples, the mean projection length was 10.4 ± 2.2 (SD) μm, with the largest measuring 17.5 μm (**Figure 2C**).

Olfactory Rod Cell Projections Can Develop in the Absence of Olfactory Cilia

As described above, olfactory rods differ from olfactory cilia in terms of size, shape, cytoskeletal composition, and distribution

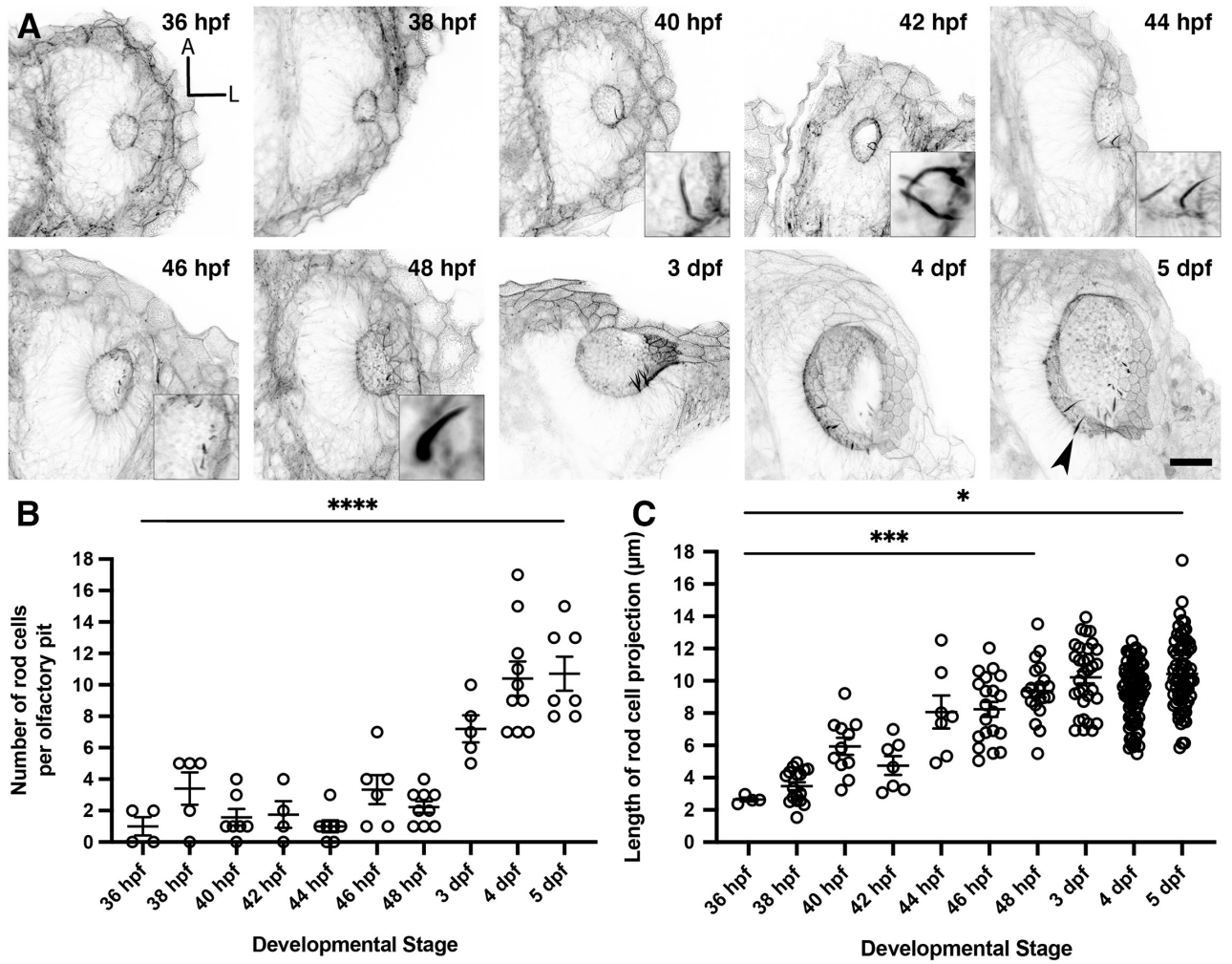

FIGURE 2 | Olfactory rod cells arise early during zebrafish olfactory pit development. **(A)** Maximum intensity projections of Airyscan confocal images showing the wild-type development of olfactory pit and olfactory rod cells at various embryonic and larval stages, using Alexa-phalloidin as a marker; anterior "A" to the top, lateral "L" to the right. Grayscale values from the original fluorescence image have been inverted. Arrowhead marks one example olfactory rod. Scale bar = 20 μm. Selected inserts show olfactory rods at higher magnification. **(B)** The change in number of olfactory rod cells per olfactory pit during embryonic development—36 hpf (*N* of olfactory pits = 4), 38 hpf (*N* = 5), 40 hpf (*N* = 7), 42 hpf (*N* = 4), 44 hpf (*N* = 7), 46 hpf (*N* = 6), 48 hpf (*N* = 9), 3 dpf (*N* = 5), 4 dpf (*N* = 10), and 5 dpf (*N* = 7). Bars indicate mean ± SEM for each stage. Linear regression analysis; ∗∗∗∗ indicates $P < 0.0001$. **(C)** The change in lengths of olfactory rod cell projections during embryonic development—36 hpf (*N* of olfactory pits = 2, *n* of olfactory rods = 4), 38 hpf (*N* = 4, *n* = 17), 40 hpf (*N* = 6, *n* = 11), 42 hpf (*N* = 3, *n* = 7), 44 hpf (*N* = 5, *n* = 7), 46 hpf (*N* = 6, *n* = 20), 48 hpf (*N* = 9, *n* = 20), 3 dpf (*N* = 5, *n* = 32), 4 dpf (*N* = 10, *n* = 82), and 5 dpf (*N* = 8, *n* = 71). Bars indicate mean ± S.E.M. for each stage. Linear regression analysis; ∗ indicates $P = 0.0251$, ∗∗∗ indicates $P = 0.0009$.

in the OE. We therefore hypothesised that olfactory rod cell projections would not be affected by mutations that disrupt the formation of cilia. To test this, we examined fish mutant for *ift88*, which codes for a component of the intraflagellar transport machinery necessary for the normal formation and maintenance of cilia (Tsujikawa and Malicki, 2004). A phalloidin stain revealed that olfactory rods were present in the OE of *ift88*$^{-/-}$ mutants at 5 dpf (**Figures 3A,B**).

The absence of cilia in *ift88*$^{-/-}$ mutants allowed us to examine morphology of the olfactory rods using scanning electron microscopy (SEM). In the phenotypically wild-type sibling OE, the olfactory rods were almost completely obscured by olfactory cilia, with only the occasional tip of a projection visible (**Figures 3C–E″**). However, SEM images of the olfactory pit of *ift88*$^{-/-}$ mutants at 4 dpf, which lack cilia, revealed the presence of rod-like projections with a similar size, number, smoothly tapering morphology, and spatial distribution to the actin-rich projections described above (**Figures 3F–I**). At their base, olfactory rods are wider in diameter (about 0.6 μm) than the olfactory cilia in wild-type larvae (0.2 μm in diameter, as is typical

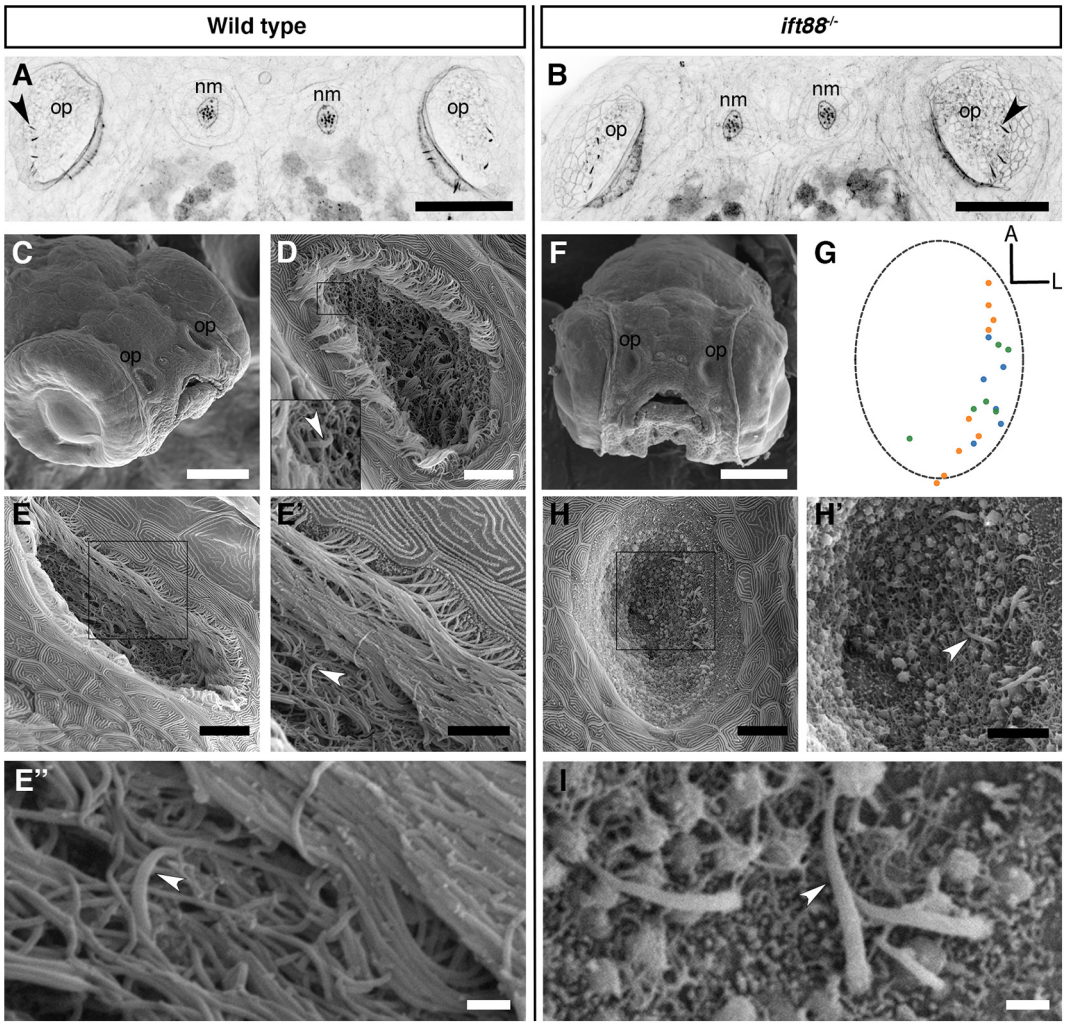

FIGURE 3 | Olfactory rod cells are present in the olfactory epithelia of *ift88*$^{-/-}$ zebrafish mutants, which lack cilia. **(A,B)** Maximum intensity projections of Airyscan confocal images of phalloidin stains of a 5 dpf wild-type **(A)** and *ift88*$^{-/-}$ mutant **(B)** larva; dorsal views, anterior to the top. Grayscale values from the original fluorescence image have been inverted. Abbreviations: nm, cranial neuromast; op, olfactory pit. Several olfactory rods (arrowheads mark examples) are visible in each olfactory pit. Scale bar = 50 μm. **(C)** SEM of the head of a 4 dpf wild-type larva. Scale bar = 100 μm. **(D,E)** SEM of 4 dpf larval wild-type olfactory pits [enlarged from panel **(C)**]. Scale bars = 10 μm. Insert in panel **(D)** shows enlarged view of boxed area in panel **(D)**. Arrowhead marks the tip of an olfactory rod cell apical projection surrounded by olfactory cilia. **(E′)** Enlarged view of boxed area in panel **(E)**. Arrowhead marks one olfactory rod. Scale bar = 5 μm. **(E″)** Enlargement of olfactory rod in panel **(E′)** (arrowhead). Scale bar = 1 μm. **(F)** Frontal view SEM of the head of a 4 dpf *ift88*$^{-/-}$ mutant larva. Scale bar = 100 μm. **(G)** A map of the positions of olfactory rod cell projection emergence through the OE in *ift88*$^{-/-}$ mutant larvae (*N* of olfactory pits = 3), based on SEM images at 4 dpf; anterior "A" to the top, lateral "L" to the right. One dot represents one olfactory rod. Different coloured dots represent olfactory rods from different larvae. (Compare with **Figure 1E**). **(H)** SEM of 4 dpf larval *ift88*$^{-/-}$ mutant olfactory pit [enlarged from panel **(F)**]. Scale bar = 10 μm. **(H′)** Enlarged view of boxed area in panel **(H)**. Arrowhead marks one example olfactory rod cell projection present despite the loss of cilia. Scale bar = 5 μm. **(I)** Enlarged SEM of olfactory rods (arrowhead marks example) in 4 dpf larval *ift88*$^{-/-}$ mutant olfactory pit (from a different individual). Scale bar = 1 μm.

for many cilia). We conclude that olfactory rods can develop in the absence of cilia.

Olfactory Rods Can Be Labelled in the Live Larva

To visualise olfactory rods in live larvae, we imaged the *Tg(actb2:Lifeact-RFP)* transgenic line at 4 and 6 dpf, and *Tg(actb2:Lifeact-GFP)* at 5 dpf (Behrndt et al., 2012). We found fluorescent apical projections in the olfactory pits of live larvae in all cases (*N* of fish = 4; **Figures 4A–C**, **Supplementary Movie 1**). These matched the size, shape, and posterolateral distribution of olfactory rod cells present in fixed samples (**Figures 4D,E**). Despite potential shrinkage due to fixation, there was no overall difference in the lengths of projections between live and fixed samples (**Figure 4E**). The zig-zag pattern exhibited by RFP-positive olfactory rods in raster-scanned images of live larvae suggested that olfactory rods were moving during image capture (**Figure 4B**). Fast-capture time series imaging of the *Tg(actb2:Lifeact-RFP)* transgenic line allowed us to observe that the projection oscillates (**Supplementary Movie 2**), possibly as a result of ciliary beating.

Neuronal Promoters Drive Reporter Expression in Olfactory Rod Cells

To test whether olfactory rod cells have features of neuronal cells, we imaged two transgenic lines that have broad neuronal expression of cytoplasmic fluorescent reporters—*Tg(Xla.tubb:jGCaMP7f)* (Chia et al., 2019) (*N* of olfactory pits = 4) and *Tg(elavl3:GCaMP6f)* (Dunn et al., 2016) (*N* = 5). Dendrites and dendritic knobs of OSNs were clearly labelled by both lines. In some examples, we observed faintly labelled projections extending from below the surface of the OE, with a similar length and morphology to olfactory rods (**Figures 5A–B′**). Imaging of double-transgenic

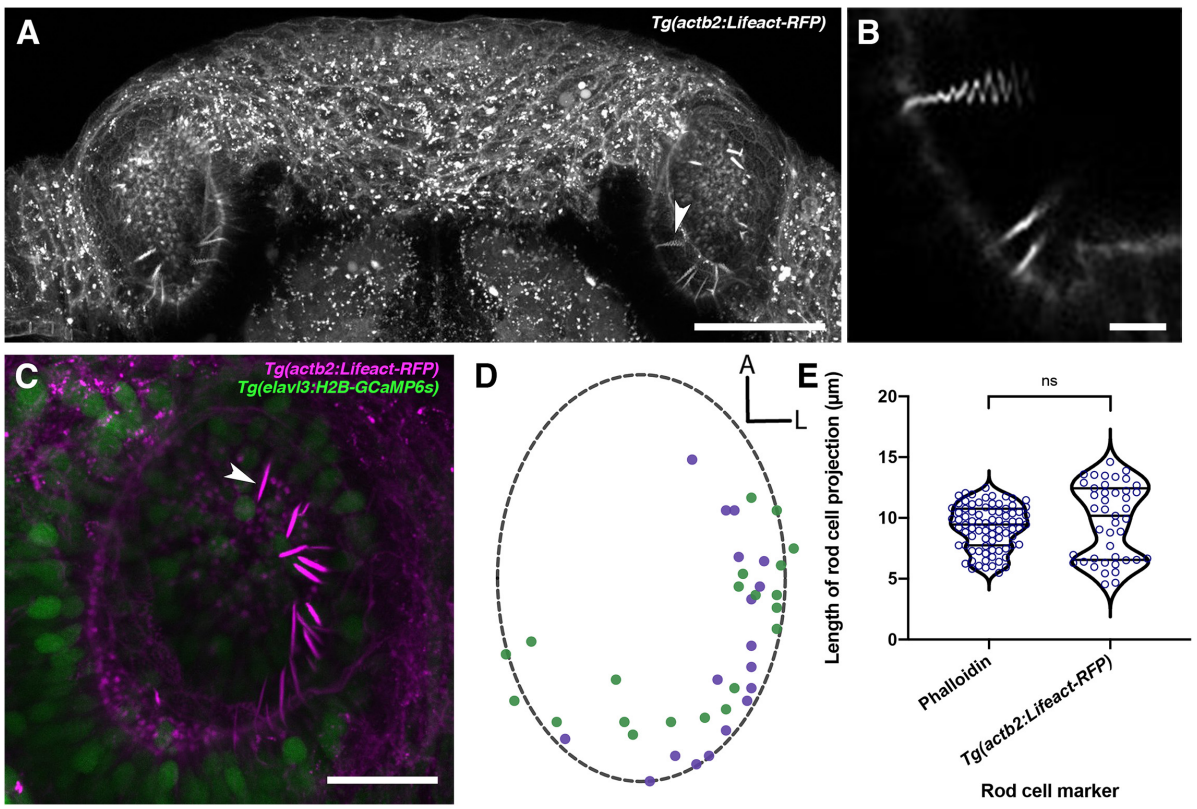

FIGURE 4 | Olfactory rods are labelled in the olfactory epithelia of live zebrafish larvae by the *Tg(actb2:Lifeact-RFP)* transgene. **(A)** Maximum intensity projection of dorsal view image of the olfactory pits of a live 6 dpf *Tg(actb2:Lifeact-RFP)* transgenic larva; anterior to the top. Arrowhead marks one example olfactory rod positive for the Lifeact-RFP transgene. Scale bar = 50 μm. **(B)** Enlargement of olfactory rods in panel **(A)** [arrowhead in panel **(A)**] oscillating during raster-scanned image capture. (Raster scanning was performed from top to bottom in the image, as it has been rotated 90° clockwise) (see **Supplementary Movie 2**). Scale bar = 5 μm. **(C)** Maximum intensity projection image of a live 4 dpf *Tg(actb2:Lifeact-RFP);Tg(elavl3:H2B-GCaMP6s)* double-transgenic larval olfactory pit; anterior to the top, lateral to the right. Arrowhead marks one example olfactory rod positive for the Lifeact-RFP transgene (magenta). Neuronal nuclei are labelled in green. Larvae were fully mounted in agarose, so olfactory rods were not moving. Scale bar = 20 μm (see **Supplementary Movie 1**). **(D)** A map of the positions of olfactory rod cell projection bases in olfactory pits of 4 dpf *Tg(actb2:Lifeact-RFP);Tg(elavl3:H2B-GCaMP6s)* double-transgenic larvae (*N* of olfactory pits = 2), based on 2D maximum intensity projections of confocal images; anterior "A" to the top, lateral "L" to the right. One dot represents one olfactory rod. Different coloured dots represent olfactory rods from different larvae, with purple corresponding to panel **(C)**. (Compare with **Figure 1E**). **(E)** A quantitative comparison of the lengths of olfactory rod cell projections in fixed larvae, using Alexa-phalloidin as a marker (*N* = 10, *n* of olfactory rods = 82) versus live larvae, using Lifeact-RFP as a marker (*N* = 2, *n* = 43). Violin plot; bars indicate the median and lower and upper quartiles for each group. Mann-Whitney *U* test; ns, not significant (*P* = 0.232).

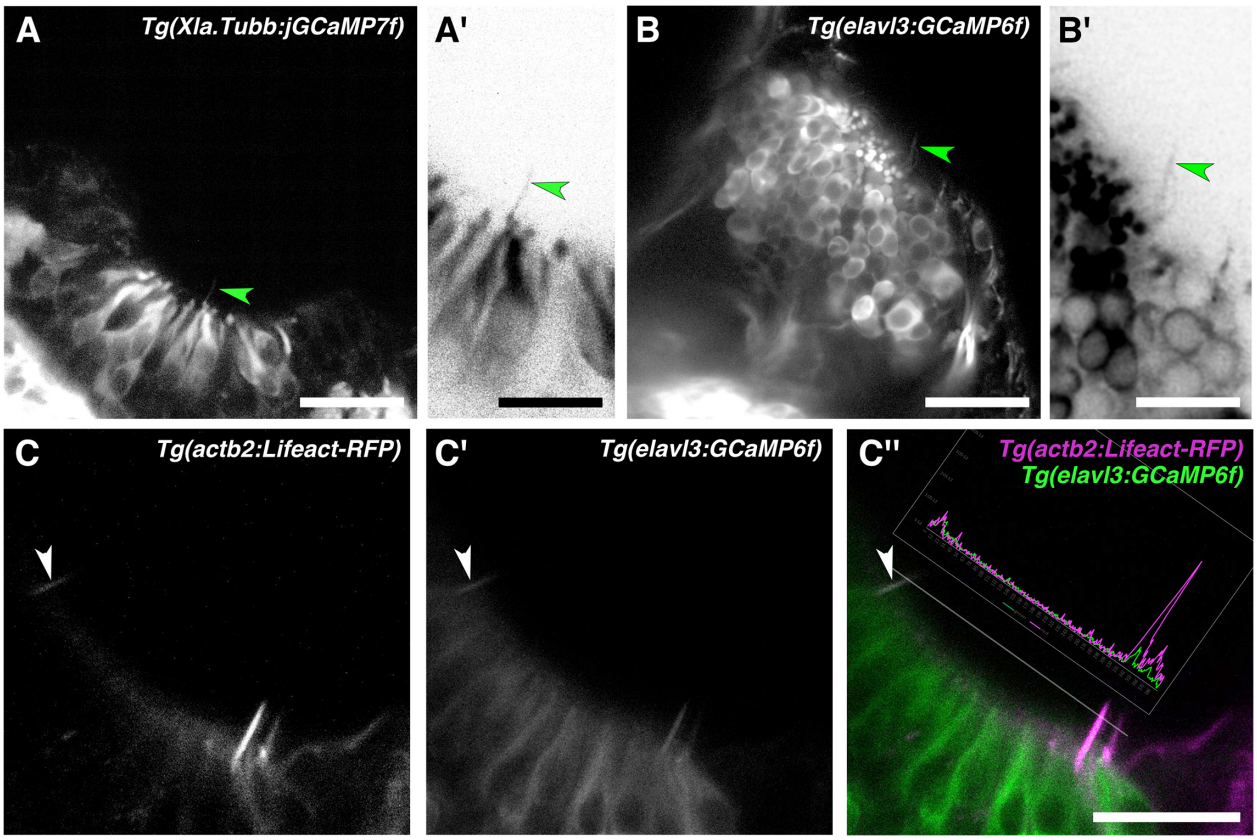

FIGURE 5 | Olfactory rod cells are labelled by the cytoplasmic neuronal markers *Tg(Xla.Tubb:jGCaMP7f)* and *Tg(elavl3:GCaMP6f)*. **(A)** Olfactory pit of a 4 dpf *Tg(Xla.Tubb:jGCaMP7f)* larva; anterior to the top, lateral to the right. Arrowhead marks one example olfactory rod, albeit faintly labelled. Scale bar = 20 μm. **(A′)** Enlargement of olfactory rod marked by arrowhead in panel **(A)** (grayscale values inverted). Scale bar = 10 μm. **(B)** Olfactory pit of a 5 dpf *Tg(elavl3:GCaMP6f)* larva; anterior to the top, lateral to the right. Arrowhead marks one example olfactory rod, albeit faintly labelled. Scale bar = 20 μm. **(B′)** Enlargement of olfactory rod marked by arrowhead in panel **(B)** (grayscale values inverted). Scale bar = 10 μm. **(C–C″)** Lifeact-RFP signal **(C)**, GCaMP6f signal **(C′)**, and merged signals **(C″)** in an olfactory pit of a 5 dpf *Tg(elavl3:GCaMP6f);Tg(actb2:Lifeact-RFP)* double-transgenic larva; anterior to the top, lateral to the right. The trace shows levels of red and green fluorescence along the dotted line, which passes through three olfactory rods positive for both Lifeact-RFP and GCaMP6f. The olfactory rod highlighted with the arrowhead shows similar levels of fluorescence in both the red and green channels. Scale bar = 20 μm.

Tg(elavl3:GCaMP6f);Tg(actb2:Lifeact-RFP) larvae at 5 dpf suggests that olfactory rod cells are GCaMP6f-positive (*N* of fish = 3; **Figures 5C–C″**). While some of the green fluorescence may be caused by bleed-through from RFP, this cannot account for all the signal, as we observed rods where the green fluorescence was detected even with dim red fluorescence (arrowhead, **Figures 5C–C″**; see trace of RFP and GCaMP6f levels); we also noted bright red pixels with no corresponding green signal. These observations suggest that olfactory rod cells may be a type of neuron.

Olfactory Rod Cells Are Not Hair-Cell-Like Cells

We initially observed the presence of olfactory rods when performing whole-mount phalloidin stains for the actin-rich stereociliary bundles of sensory hair cells in the inner ear and lateral line. Given the superficial similarity in appearance of olfactory rods to hair-cell stereocilia in low-magnification phalloidin stains (see, for example, **Figure 3A**), and a report of a rare cell type bearing stereocilia-like microvilli in the rat OE (Menco and Jackson, 1997), we were interested to test whether there is any similarity between olfactory rod cells and mechanosensory hair cells of the inner ear and lateral line. As shown in **Figures 1** and **3**, the zebrafish olfactory rod appears to be a single structure rather than a collection of microvilli or stereocilia. To test whether olfactory rod cells express sensory hair cell markers, we performed an Alexa-phalloidin co-stain on the *Tg(pou4f3:GFP)* transgenic line, a known marker for hair cells (Xiao et al., 2005). At 5 dpf, the stereociliary bundle of lateral line neuromast hair cells was clearly marked by both GFP and phalloidin, which acted as our positive control (**Figures 6A–A″**). However, the GFP did not co-localise with the phalloidin signal in the olfactory rods, or in the cell body beneath a phalloidin-positive olfactory rod (**Figures 6B–B″**).

Mechanosensory hair cells, including those of the zebrafish lateral line, are susceptible to oxidative damage by aminoglycoside antibiotics, which can preferentially enter hair cells via mechanotransduction channels, and cause cell death

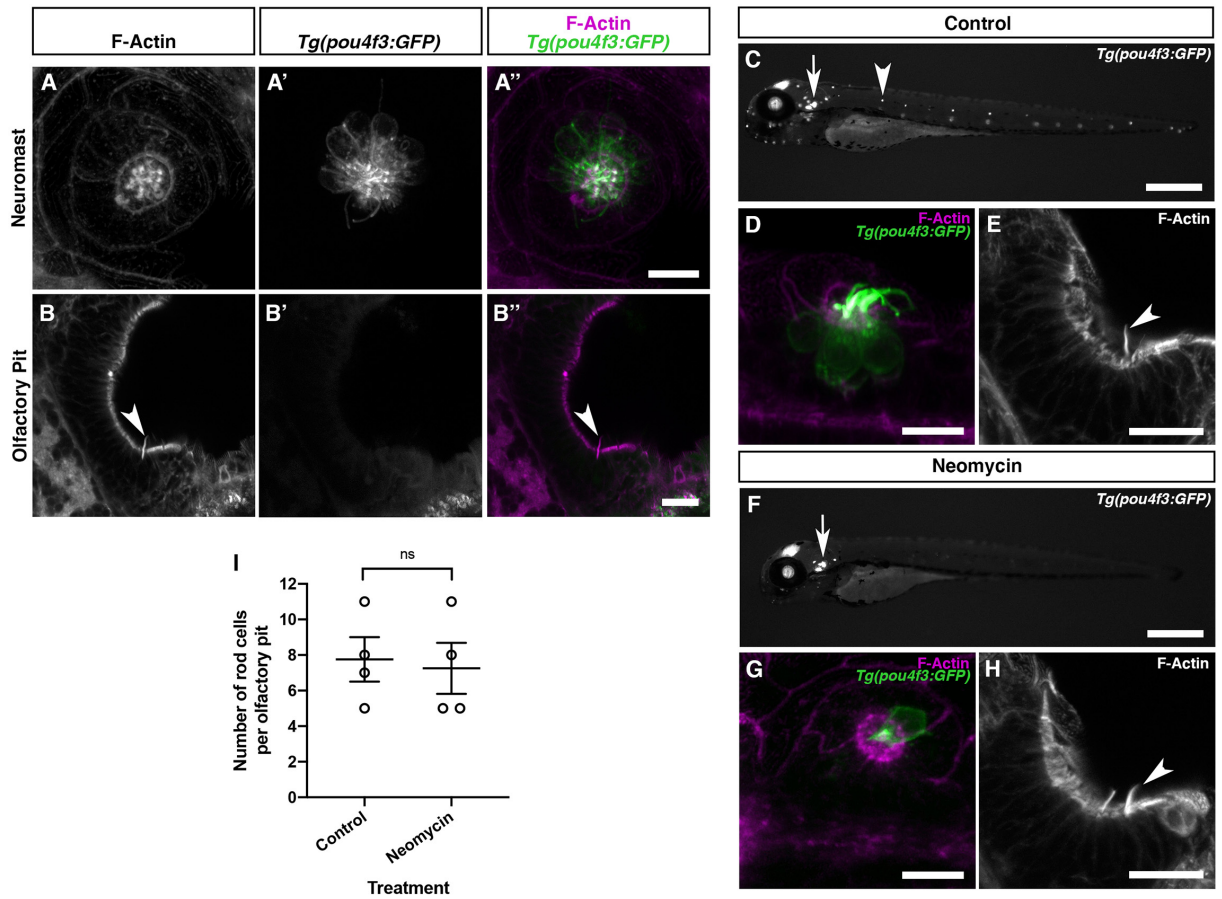

FIGURE 6 | Olfactory rod cells in the zebrafish olfactory epithelium are not hair-cell-like. **(A–A″)** Maximum intensity projection of Airyscan confocal image of Alexa-phalloidin signal **(A)**, *Tg(pou4f3:GFP)* signal **(A′)**, and merged signals **(A″)** in a cranial neuromast of a 5 dpf larva. Scale bar = 10 μm. **(B–B″)** Airyscan confocal image of Alexa-phalloidin signal **(B)**, *Tg(pou4f3:GFP)* signal **(B′)**, and merged signals **(B″)** in an olfactory pit of a 5 dpf larva; anterior to the top, lateral to the right. Arrowhead marks one olfactory rod. Scale bar = 20 μm. **(C,F)** Widefield imaging of 3 dpf *Tg(pou4f3:GFP)* larvae showing the damaging effects of 500 μM neomycin treatment for 60 min on lateral line neuromast hair cells. Fluorescence is lost or greatly reduced in both trunk (arrowhead) and cranial neuromasts, whereas fluorescence in hair cells of the inner ear maculae and cristae (arrow) is unaffected. Scale bars = 500 μm. **(D,G)** Maximum intensity projections of Airyscan confocal images showing the damaging effects of 500 μM neomycin treatment for 60 min on hair cells in a cranial neuromast of a 3 dpf larva, using *Tg(pou4f3:GFP)* (green) and Alexa-phalloidin (magenta) as markers. Scale bars = 10 μm. **(E,H)** Maximum intensity projections of Airyscan confocal images showing no effect of 500 μM neomycin treatment for 60 min on olfactory rods, using Alexa-phalloidin as a marker; anterior to the top, lateral to the right. Arrowheads mark olfactory rods. Scale bars = 20 μm. **(I)** The number of olfactory rod cell projections per olfactory pit of 3 dpf *Tg(pou4f3:GFP)* larvae after 500 μM neomycin treatment for 60 min (*N* of olfactory pits = 4), compared with an untreated group (*N* = 4). Bars indicate mean ± SEM. Welch's unpaired two-tailed *t*-test; ns, not significant (*P* = 0.8018).

following a calcium flux and release of reactive oxygen species by mitochondria (Esterberg et al., 2013, 2016; Pickett et al., 2018). To test whether olfactory rod cells are similarly sensitive, we investigated whether treatment with the aminoglycoside neomycin has the same damaging effect on olfactory rod cells as on lateral line hair cells. Following neomycin treatment at 500 μM for 60 min on 3 dpf *Tg(pou4f3:GFP)* larvae, lateral line hair cells were lost or severely damaged, as determined by a decrease in the number of GFP-positive cells (together with loss of their phalloidin-positive stereocilia) in both cranial and trunk neuromasts and a change in morphology of any remaining cells (**Figures 6C,D,F,G**). By contrast, olfactory rods appeared unaffected (**Figure 6E,H**), with no significant change in the number of olfactory rods present in each olfactory pit (**Figure 6I**). Taken together, the smooth appearance of the olfactory rods, lack of hair cell marker expression, and resistance to neomycin indicate that olfactory rod cells are not closely related to hair cells.

A Sub-population of Olfactory Rod Cells Expresses a Lifeact Transgene Driven by the *sox10* Promoter

Sox10 is a known marker of both neural crest and otic epithelium (Dutton et al., 2001). Robust transgene expression driven by the *sox10* promoter has been reported in the OE and other tissues in the zebrafish (Mongera et al., 2013; Saxena et al., 2013). We have generated a *Tg(sox10:Lifeact-mRFPruby)* transgenic line to visualise actin localisation and dynamics in the live embryo in *sox10*-expressing tissues. As reported for the

Tg(sox10:eGFP) transgene (Saxena et al., 2013), we observed OSNs expressing *Tg(sox10:Lifeact-mRFPruby)* in the OE at 4 and 5 dpf; based on morphology, most of these cells were microvillous OSNs. However, staining with Alexa-phalloidin on fixed samples revealed the co-expression of Lifeact-mRFPruby in a sub-population of phalloidin-positive olfactory rod cell projections (**Figures 7A–B″**). Not all olfactory rod cells expressed the transgene; an average of 64.4% of olfactory rod cells marked by phalloidin (*N* of olfactory pits = 5, *n* of olfactory rods = 59) also expressed Lifeact-mRFPruby (**Figure 7C**). As for the olfactory rods labelled with Lifeact-RFP, rods labelled with Lifeact-mRFPruby oscillated (**Supplementary Movie 3**).

The sparse expression of the *Tg(sox10:Lifeact-mRFPruby)* transgene allowed us to visualise the morphology of the cell body of olfactory rod cells and ask whether they have an axon. Lifeact-mRFPruby-expressing cell bodies were positioned apically in the OE and were rounded in shape (**Figures 7B–B″,E**). They were morphologically distinct from the well-described microvillous OSNs (**Figures 7D,E**) as well as ciliated and crypt OSNs. The axons of microvillous OSNs were visible in those cells labelled by the transgene (**Figure 7D**). However, with this marker, we were unable to observe an axon extending from the cell body of olfactory rod cells (*N* of olfactory pits = 5, *n* of cells = 9; **Figure 7E**).

To test whether the development of olfactory rod cells is dependent on *sox10* function, we stained $sox10^{-/-}$ homozygous mutants (Dutton et al., 2001) with Alexa-phalloidin. Olfactory rods were present in $sox10^{-/-}$ mutants at 5 dpf, but variable in number (*N* of olfactory pits = 8, *n* of olfactory rods = 53; **Figure 8**). Taken together, the data from *Tg(sox10:Lifeact-mRFPruby)* transgenic and $sox10^{-/-}$ mutant larvae indicate that *sox10* function is not essential for the formation of olfactory rod cells.

DISCUSSION

The zebrafish is a key model organism for the study of the olfactory system (reviewed in Kermen et al., 2013; Calvo-Ochoa and Byrd-Jacobs, 2019), and a complete inventory of the cell types present in the zebrafish OE will be an important resource and reference point for further study. Through the use of phalloidin staining, immunohistochemistry, transgenic zebrafish lines, SEM and high-resolution fluorescence confocal imaging, we have identified a rare cell type, the olfactory rod cell, in the zebrafish larval and juvenile OE. Olfactory rod cells, which have not previously been described in zebrafish to our knowledge, are morphologically distinct from the well-characterised OSNs and other known cell types in terms of their apical projections, cell shape, and distribution and positioning within the OE.

The Olfactory Rod: An Actin-Rich Apical Projection

The spectacular actin-rich projection of the olfactory rod cell adds to the rich repertoire of known F-actin-based cellular specialisations, which include microvilli, stereocilia, lamellipodia, filopodia, cytonemes and microridges (reviewed in Heath and Holifield, 1991; Theriot and Mitchison, 1991; Ramírez-Weber and Kornberg, 1999; Pinto et al., 2019; Inaba et al., 2020). Many sensory cell types, in both fish and mammals, bear actin-rich mechano- or chemosensory microvillous projections, including the stereocilia of sensory hair cells (Tilney et al., 1980; reviewed in Gillespie and Müller, 2009; Barr-Gillespie, 2015), and the microvilli of olfactory and vomeronasal microvillous neurons, SCCs of the skin and barbel (Kotrschal et al., 1997; Finger et al., 2003; Hansen and Finger, 2008), taste bud cells (Hansen et al., 2002; Zachar and Jonz, 2012), spinal cerebrospinal fluid-contacting neurons (CSF-cNs; Djenoune et al., 2014; Desban et al., 2019), Merkel cells, retinal Müller glia (Sekerková et al., 2004), and the brush and tuft cells of mammalian respiratory and intestinal epithelia, respectively (reviewed in Reid et al., 2005; Schneider et al., 2019). As a single structure with a smoothly tapering morphology, the zebrafish olfactory rod differs from these oligovillous structures. Adult zebrafish SCCs, found distributed over the entire body surface (Kotrschal et al., 1997), and mature light cells of the zebrafish taste bud (Hansen et al., 2002) each bear a single microvillus, but at 1–3 μm in length, these are much shorter than the olfactory rods we describe.

Olfactory rod cells are distinct from rodlet cells, which have been reported in many different epithelial tissues of marine and freshwater fish, including zebrafish, and contain several intracellular electron-dense rodlets within a thick cuticular-like wall (Bannister, 1966; reviewed in Morrison and Odense, 1978; Hansen and Zeiske, 1998; Dezfuli et al., 2007; DePasquale, 2020). Recently, phalloidin staining has demonstrated that the rodlets, which can be extruded from the cell, are not composed of F-actin (DePasquale, 2020). Thus, zebrafish olfactory rod cells, which are unique to the OE at the larval stages we have described, are not related to rodlet cells.

Olfactory Rod Cells in Other Teleost Species

Previous studies have provided descriptions of cell types similar to the olfactory rod cell in other teleost species, including the common minnow (Bannister, 1965), several eel species (Schulte, 1972; Yamamoto and Ueda, 1978), goldfish (Breipohl et al., 1973; Ichikawa and Ueda, 1977), rainbow trout (Rhein et al., 1981), common bleak (Hernádi, 1993), catfish (Datta and Bandopadhyay, 1997), and several cave fish and cave loach species (Waryani et al., 2013, 2015; Zhang et al., 2018).

Using transmission electron microscopy (TEM), Bannister (1965) reported sparsely populated rod-shaped protrusions, approximately 4 μm in length and shorter than surrounding sensory and non-sensory olfactory cilia, in the OE of adult (3.7 cm) common minnow (*Phoxinus phoxinus*). Here, the rod-like projection consisted of several bundles of fibres, consistent with the appearance of F-actin, extending from deep within the cell (Bannister, 1965). Similarly, using TEM and SEM respectively, Schulte (1972) and Yamamoto and Ueda (1978) reported the presence of olfactory rod cells in the OE of several adult eel species: European eel (*Anguilla anguilla*), Japanese eel (*A. japonica*), white-spotted conger (*Conger myriaster*), buffoon snake eel (*Microdonophis erabo*), and brutal moray

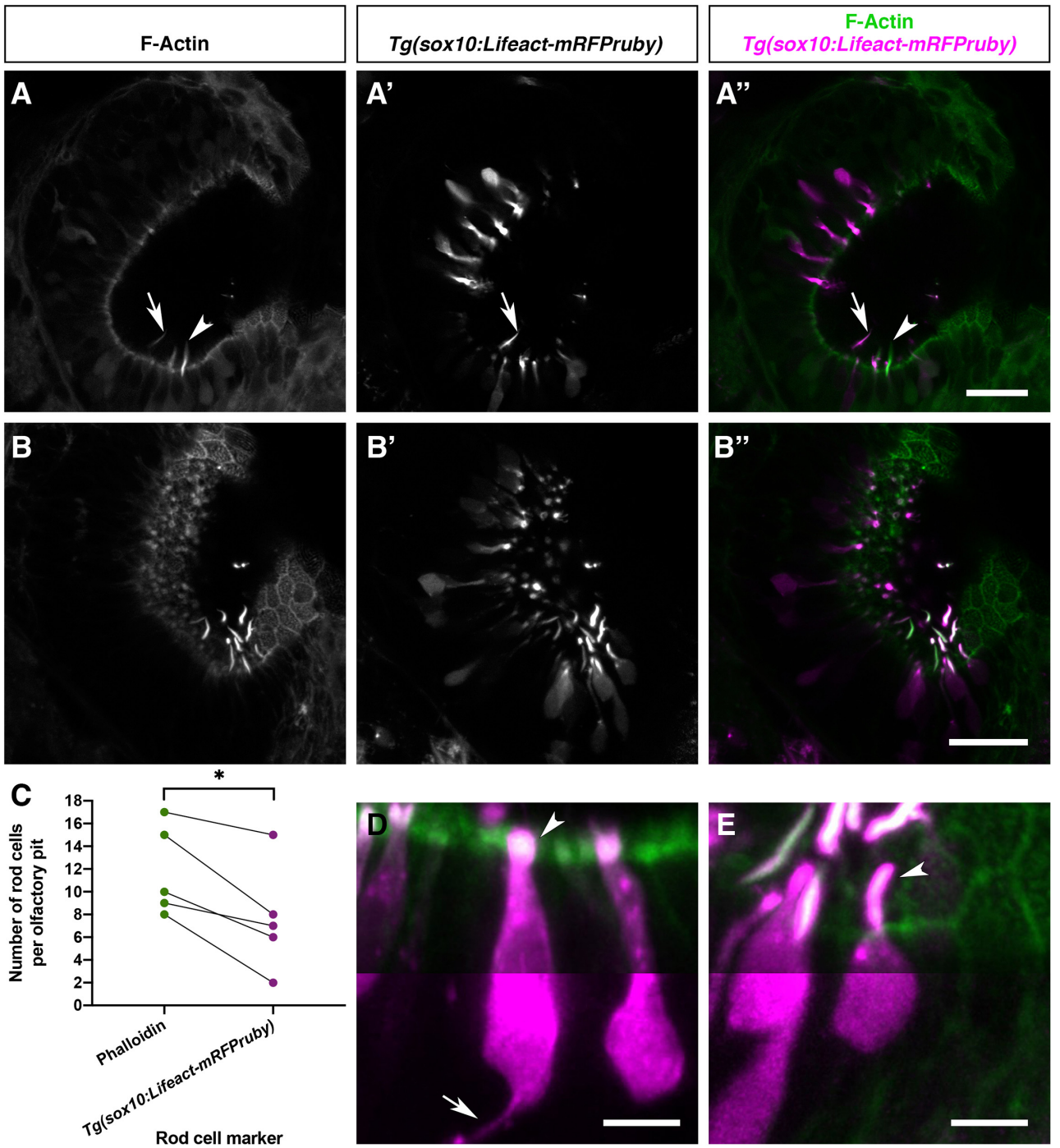

FIGURE 7 | Olfactory rod cells are apically located in the zebrafish olfactory epithelium, with a rounded cell body and no detectable axon. **(A–B″)** Airyscan confocal image of Alexa-phalloidin signal **(A,B)**, *Tg(sox10:Lifeact-mRFPruby)* signal **(A′,B′)**, and merged signals **(A″,B″)** in olfactory pits of 4–5 dpf larvae; anterior to the top, lateral to the right. Arrowhead marks one olfactory rod negative for Lifeact-mRFPruby. Arrow marks one olfactory rod positive for Lifeact-mRFPruby. Scale bars = 20 μm. **(C)** Number of olfactory rod cells positively marked by Alexa-phalloidin (*n* of olfactory rods = 59), compared with the number of those also marked by *Tg(sox10:Lifeact-mRFPruby)* (*n* = 38), in olfactory pits of 4–5 dpf larvae (*N* of olfactory pits = 5). Connecting lines indicate olfactory rods from the same olfactory pit. Paired two-tailed *t*-test; ∗ indicates $P = 0.0146$. **(D)** Enlargement of two microvillous OSNs, expressing Lifeact-mRFPruby, in the OE of a 4 dpf larva; Alexa-phalloidin signal (green), *Tg(sox10:Lifeact-mRFPruby)* signal (magenta). Arrowhead marks the microvillous apical projections. The gamma value for the magenta channel in the bottom half of the panel has been set to 0.5 to show the axon from one of the cells (arrow). Scale bar = 5 μm. **(E)** Enlargement of olfactory rod cells (of which both the apical actin projections and cell bodies are labelled by the *Tg(sox10:Lifeact-mRFPruby)* transgene) in the OE of a 4 dpf larva; Alexa-phalloidin signal (green), *Tg(sox10:Lifeact-mRFPruby)* signal (magenta). Arrowhead marks an olfactory rod cell apical projection, positive for both markers. The gamma value for the bottom half of the panel has been set to 0.5 as in panel **(D)**; no axon is visible. Scale bar = 5 μm. See also **Supplementary Movie 3**.

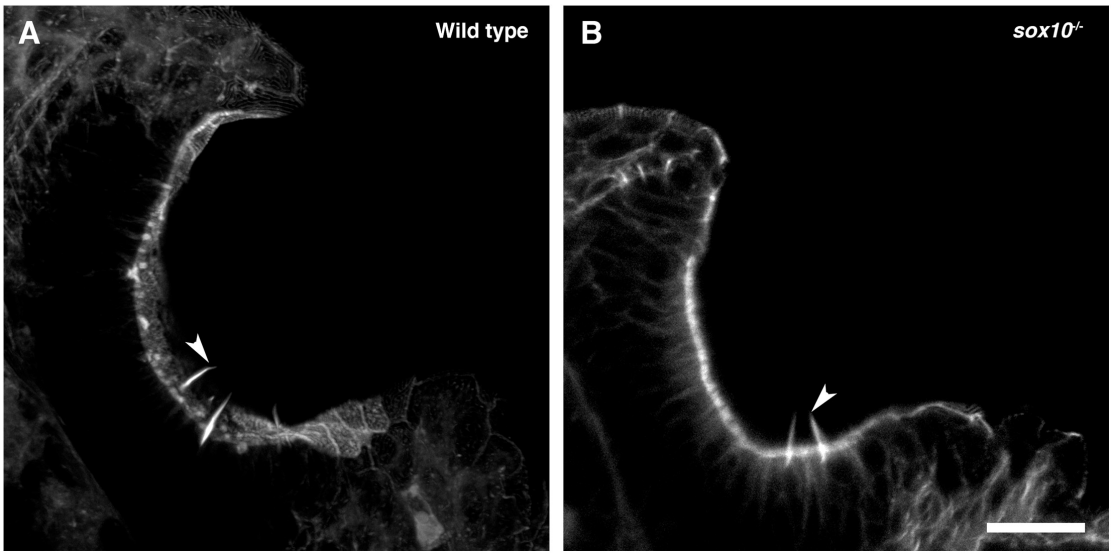

FIGURE 8 | Olfactory rod cells are present in the olfactory epithelia of *sox10*$^{-/-}$ zebrafish mutants. **(A)** Maximum intensity projection of Airyscan confocal image of phalloidin stain in a 5 dpf larval wild-type olfactory pit; anterior to the top, lateral to the right. Arrowhead marks one example olfactory rod. Scale bar = 20 μm. **(B)** Airyscan confocal image of phalloidin stain in a 5 dpf larval *sox10*$^{-/-}$ mutant olfactory pit; anterior to the top, lateral to the right. Arrowhead marks one example olfactory rod. Scale bar = 20 μm.

(*Gymnothorax kidako*). In European eels, the cells were described as a receptor with a single rod-shaped appendage, measuring 0.8 μm in diameter and extending 4 μm above the apical surface of the epithelium (Schulte, 1972). Olfactory rods in the other four species measured 1 μm in diameter and 10 μm in length. Olfactory rods were either found to exist solitarily or in a group; interestingly, it was noted that olfactory cilia were sparse in areas where olfactory rods occurred in a group (Yamamoto and Ueda, 1978).

More recent reports include comparisons of the surface structures of olfactory epithelia in different adult cave fish and loaches. SEMs in *Sinocyclocheilus jii* and *S. furcodorsalis* cave fish, and in *Oreonectes polystigmus* and *O. guananensis* cave loaches revealed that olfactory rods were clustered in different regions of olfactory rosette lamellae (Waryani et al., 2013, 2015). Another SEM study on the variations in olfactory systems of adult cave fish species of different habitats reported not just one, but three different cell types all classified as "rod cilia" in the olfactory epithelia of *S. anshuiensis* and *S. tianlinensis*. The first cell type had a long base with an oval apex, the second contained an oval base with a thin apex, while the third was rod-shaped and thin from base to tip, measuring 2.01–3.08 μm in length (Zhang et al., 2018). Despite the shorter length, this third type appeared morphologically consistent with zebrafish olfactory rod cells. Unlike other teleosts, olfactory rod cells were reported as the dominant cell type over ciliated and microvillous OSNs in the OE of *S. jii* (Waryani et al., 2013). This may be an example of the known compensatory enhancement of the olfactory system in blind morphs of cave fish (Bibliowicz et al., 2013; reviewed in Krishnan and Rohner, 2017).

Although there appear to be variations in the numbers and sizes of olfactory rod cells reported in these other teleost species, some of these cells may be homologous to the olfactory rod cells we describe in zebrafish larvae. However, all of these previous studies were limited to fixed adult samples by means of TEM and SEM, and none have tested or confirmed the cytoskeletal composition of the olfactory rod.

Olfactory Rod Cells Differ From Known Olfactory Sensory Neurons

We have detected weak expression of cytoplasmic fluorescent markers driven by neuronal promoters in olfactory rod cells. However, we were unable to detect an axon in nine individual olfactory rod cells imaged with a Lifeact-mRFPruby transgene at 4–5 dpf. Of note, Ichikawa and Ueda (1977) performed olfactory nerve bundle transection in adult goldfish to determine which cell types are OSNs. As expected, transection caused retrograde degeneration of both ciliated and microvillous OSNs. Olfactory rod cells, however, were still identifiable by SEM in the OE 10 days after nerve transection. The authors concluded that adult goldfish olfactory rod cells are not OSNs. This is similar to the observation that OB ablation did not lead to death of a subset of microvillous cells in the rat OE (Carr et al., 1991). It now appears that such microvillous cells are a class of sensory paraneuron, as they are cholinergic and express components of the taste transduction pathway (Genovese and Tizzano, 2018). Whether olfactory rod cells express similar genes remains to be determined.

Zebrafish Olfactory Rod Cells Are Not Artefacts

Since the first report of olfactory rod cells, several studies have proposed that they may represent senescent forms of OSNs or fixation artefacts (Muller and Marc, 1984; Moran et al., 1992;

reviewed in Hansen and Zielinski, 2005). A study in the goldfish (*Carassius auratus*) and channel catfish (*Ictalurus punctatus*), using TEM, SEM and filling with horseradish peroxidase, concluded that olfactory rods are most likely a result of fusion of olfactory cilia or microvilli—an indicator of ageing OSNs (Muller and Marc, 1984). A later study on the ultrastructure of olfactory mucosa in brown trout (*Salmo trutta*) also classified olfactory rods as products of the fusion of olfactory cilia during fixation (Moran et al., 1992). Indeed, TEM images in this study showed multiple ciliary axonemes surrounded by a single membrane (Moran et al., 1992). The presence of such fixation artefacts has led to frequent dismissal of olfactory rod cells in the literature, for example in juvenile and adult European eels (Sola et al., 1993). In the zebrafish, however, the olfactory rods we describe are clearly not a fixation artefact, as they are present in the live larva. Moreover, they are not formed by fusion of cilia, as the olfactory rods are F-actin-positive, do not stain with an anti-acetylated α-tubulin antibody, and are present in *ift88*$^{-/-}$ mutants which lack cilia.

Possible Functions of Olfactory Rod Cells

Actin-rich projections on sensory cells are known to have mechanosensory (reviewed in Gillespie and Müller, 2009), chemosensory (Höfer and Drenckhahn, 1999; Hansen et al., 2002; Zachar and Jonz, 2012), or multimodal functions (for example in CSF-cNs in zebrafish; Djenoune et al., 2014; Desban et al., 2019). A mechanosensory role for zebrafish olfactory rod cells, for example in detecting ciliary movement or ciliary-driven fluid flow, or a chemosensory role in detecting odorants, could aid olfactory perception in the larva. They may function similarly to microvillous cells that lack axons in the mammalian OE, and participate in volume release for local modulation of OSNs or non-sensory cells (Genovese and Tizzano, 2018), thereby acting as paraneurons (reviewed in Fujita, 1989). The activity of the *tubb* promoter in olfactory rod cells is consistent with this interpretation, as expression of neuronal tubulin has previously been detected in paraneurons (Iwanaga et al., 1982). Another possibility is that olfactory rod cells could correspond to brush or tuft cells in air-breathing mammals, which have important roles in immunity (Andres, 1975; reviewed in Reid et al., 2005; Howitt et al., 2016; reviewed in Schneider et al., 2019). These ideas remain to be tested.

Possible Origins of Olfactory Rod Cells

Our work does not address the developmental origin of olfactory rod cells, but it is of interest that they express a *sox10*-driven transgene, albeit in a mosaic fashion. *Sox10* mRNA is frequently described as a neural crest marker, but is also expressed strongly in otic epithelium (Dutton et al., 2001), a placodally derived tissue. The use of *sox10*-driven transgenic lines to identify neural crest derivatives remains controversial. Expression of a *sox10*:eGFP transgene together with photoconversion studies has led to the conclusion that a subpopulation of microvillous OSNs in the OE is derived from neural crest (Saxena et al., 2013), and use of an inducible *sox10*:*ER*^{T2}-*Cre* transgenic line has identified previously "contested" neural crest derivatives, including cells in the sensory barbels (Mongera et al., 2013). However, using lineage reconstruction through backtracking and photoconversion experiments, Aguillon et al. (2018) have argued that all olfactory neurons, including OSNs and gonadotropin-releasing hormone 3 (GnRH3) cells, are derived entirely from preplacodal progenitors. Given this controversy, we are unable to conclude whether olfactory rod cells are derived from the placode or neural crest.

The *Tg(sox10:Lifeact-mFRPruby)* line is expressed in a subset of both olfactory rod cells and of microvillous OSNs, with variation in the proportion of expressing cells between individuals. This could reflect true heterogeneity in the olfactory rod cell and microvillous OSN populations, or it could be a result of mosaic or leaky expression of the transgene. Mosaic expression is typical for many transgenes (Mosimann et al., 2013), while leaky expression, which can be explained through the lack of appropriate silencer elements (Jessen et al., 1999), is suspected for the *sox10* promoter fragment used in our transgenic construct (reviewed in Tang and Bronner, 2020). Nevertheless, the *Tg(sox10:Lifeact-mRFPruby)* line has proved a fortuitous tool for visualising olfactory rod cells in the live larva.

Concluding Remarks

A detailed understanding of the vertebrate olfactory system is important both from a cellular and developmental perspective and for its clinical relevance. Olfactory dysfunction can signify underlying cellular disorders and can also be implicated in neurodegenerative diseases (reviewed in Whitlock, 2015; Bergboer et al., 2018). OSNs project directly to the OB, and thus provide an entry route for pathogens to the brain (reviewed in Dando et al., 2014). Cells in the OE can themselves be damaged by viral infection, leading to a reduction, change, or loss of sense of smell (Brann et al., 2020; Gupta et al., 2020; Kraus et al., 2020). The identification of zebrafish olfactory rod cells, with their unique flexible actin-rich protrusion, offers new opportunities to explore the biology of these cells in a genetically tractable model organism, and thus to understand their contribution to the multimodal sensory functions of the vertebrate olfactory epithelium.

DATA AVAILABILITY STATEMENT

The raw data supporting the conclusions of the article will be made available at Figshare, doi: 10.6084/m9.figshare.13710100.

ETHICS STATEMENT

The animal study was reviewed and approved by ethics committees in Sheffield and Singapore. All zebrafish work in Sheffield was reviewed by the Project Applications and Amendments Committee of the Animal Welfare and Ethical Review Body (AWERB), and undertaken under licence from the UK Home Office, according to recommended

standard husbandry conditions (Aleström et al., 2019). All experiments in Singapore were performed under guidelines approved by the Institutional Animal Care and Use Committee of Biopolis (#181408).

AUTHOR CONTRIBUTIONS

KYC, TW, and SJ: designed the research, data analysis. KYC, SJ, TW, SB, NvH, MM, and CH: conducted the experiments. KYC and TW: writing (original draft). KYC, TW, and SJ, with additional contributions from SB, NvH, and CH: writing (review and editing). All authors contributed to the article and approved the submitted version.

FUNDING

KYC was funded by an A*STAR Research Attachment Programme Ph.D. studentship (ARAP-2019-01-0014). Research in Sheffield was supported by a BBSRC project grant (BB/S007008/1) to TW and SB. Imaging in Sheffield was carried out in the Sheffield Electron Microscopy Unit and Wolfson Light Microscopy Facility, with support from a BBSRC ALERT14 award (BB/M012522/1) to TW and SB for light-sheet microscopy. Work in the SJ lab was funded by a start-up grant from the Lee Kong Chian School of Medicine, Nanyang Technological University, Singapore.

ACKNOWLEDGMENTS

We thank Karen Camargo-Sosa and Robert Kelsh for providing fixed *sox10*$^{-/-}$ larvae. We thank Henry Roehl for making the p5E *-4725 sox10* promoter (originally from the Kelsh lab), *Lifeact-mRFPruby* construct (originally from the Wedlich-Söldner and Sixt labs), and Zeiss Axio Zoom.V16 microscope available to us, Ana Almeida Jones for help with imaging, Emily Glendenning for technical support, and members of the Whitfield lab for discussion. We are grateful to the Sheffield Aquarium Team for excellent fish care. We also thank Kathleen Cheow, Ruey-Kuang Cheng, Jason Lai, and Tim Saunders for assistance with fish in Singapore.

SUPPLEMENTARY MATERIAL

The Supplementary Material for this article can be found online at: https://www.frontiersin.org/articles/10.3389/fphys.2021.626080/full#supplementary-material

Supplementary Movie 1 | Olfactory rods are labelled in the olfactory epithelia of live zebrafish by the *Tg(actb2:Lifeact-RFP)* transgene. 3D rendering of a confocal image of a 4 dpf *Tg(actb2:Lifeact-RFP)*;*Tg(elavl3:H2B-GCaMPs)* double-transgenic larval olfactory pit; anterior to the top. Olfactory rods are labelled in magenta; neuronal nuclei are labelled in green.

Supplementary Movie 2 | Olfactory rods labelled with Lifeact-RFP in the olfactory epithelia of live zebrafish larvae oscillate. Fast-capture time series confocal imaging (5.98 frames per second, fps) of olfactory rods in a 6 dpf *Tg(actb2:Lifeact-RFP)* larva; anterior to the top, lateral to the left. Playback speed of the movie is 6 fps. Scale bar = 10 μm.

Supplementary Movie 3 | Olfactory rods labelled with Lifeact-mRFPruby in the olfactory epithelia of live zebrafish larvae oscillate. Fast-capture time series light-sheet imaging (50.04 fps) of a 5 dpf *Tg(sox10:Lifeact-mRFPruby)* larval olfactory pit; anterior to the top left, lateral to the top right. Beating olfactory cilia are visible in brightfield (grayscale), and oscillating olfactory rods are labelled by Lifeact-mRFPruby (magenta). Playback speed of the movie is 7 fps. Scale bar = 20 μm.

REFERENCES

Aguillon, R., Batut, J., Subramanian, A., Madelaine, R., Dufourcq, P., Schilling, T. F., et al. (2018). Cell-type heterogeneity in the early zebrafish olfactory epithelium is generated from progenitors within preplacodal ectoderm. *Elife* 7:e32041. doi: 10.7554/eLife.32041

Ahuja, G., Nia, S. B., Zapilko, V., Shiriagin, V., Kowatschew, D., Oka, Y., et al. (2014). Kappe neurons, a novel population of olfactory sensory neurons. *Sci. Rep.* 4:4037. doi: 10.1038/srep04037

Aleström, P., D'Angelo, L., Midtlyng, P. J., Schorderet, D. F., Schulte-Merker, S., Sohm, F., et al. (2019). Zebrafish: Housing and husbandry recommendations. *Lab. Anim.* 0, 1–12. doi: 10.1177/0023677219869037

Andres, K. H. (1975). Neue morphologische grundlagen zur physiologie des riechens und schmeckens. *Arch. Otorhinolaryngol.* 210, 1–41. doi: 10.1007/BF00453706

Axel, R. (1995). The molecular logic of smell. *Sci. Am.* 273, 154–159. doi: 10.1038/scientificamerican1095-154

Bannister, L. H. (1965). The fine structure of the olfactory surface of teleostean fishes. *Q. J. Microsc. Sci.* 106, 333–342.

Bannister, L. H. (1966). Is *Rhabdospora thelohani* (Laguesse) a sporozoan parasite or a tissue cell of lower vertebrates? *Parasitology* 56, 633–638. doi: 10.1017/S0031182000071651

Barr-Gillespie, P.-G. (2015). Assembly of hair bundles, an amazing problem for cell biology. *Mol. Biol. Cell* 26, 2727–2732. doi: 10.1091/mbc.E14-04-0940

Behrndt, M., Salbreux, G., Campinho, P., Hauschild, R., Oswald, F., Roensch, J., et al. (2012). Forces driving epithelial spreading in zebrafish gastrulation. *Science* 338, 257–260. doi: 10.1126/science.1224143

Bergboer, J. G. M., Wyatt, C., Austin-Tse, C., Yaksi, E., and Drummond, I. A. (2018). Assaying sensory ciliopathies using calcium biosensor expression in zebrafish ciliated olfactory neurons. *Cilia* 7:2. doi: 10.1186/s13630-018-0056-1

Bettini, S., Milani, L., Lazzari, M., Maurizii, M. G., and Franceschini, V. (2017). Crypt cell markers in the olfactory organ of *Poecilia reticulata*: analysis and comparison with the fish model *Danio rerio*. *Brain Struct. Funct.* 222, 3063–3074. doi: 10.1007/s00429-017-1386-2

Bibliowicz, J., Alié, A., Espinasa, L., Yoshizawa, M., Blin, M., Hinaux, H., et al. (2013). Differences in chemosensory response between eyed and eyeless *Astyanax mexicanus* of the Rio Subterráneo cave. *Evodevo* 4:25. doi: 10.1186/2041-9139-4-25

Biechl, D., Tietje, K., Gerlach, G., and Wullimann, M. F. (2016). Crypt cells are involved in kin recognition in larval zebrafish. *Sci. Rep.* 6:24590. doi: 10.1038/srep24590

Brann, D. H., Tsukahara, T., Weinreb, C., Lipovsek, M., Van den Berge, K., Gong, B., et al. (2020). Non-neuronal expression of SARS-CoV-2 entry genes in the olfactory system suggests mechanisms underlying COVID-19-associated anosmia. *Sci. Adv.* 6:eabc5801. doi: 10.1126/sciadv.abc5801

Breipohl, W., Bijvank, G. J., and Zippel, H. P. (1973). Rastermikroskopische untersuchungen der olfaktorischen rezeptoren im riechepithel des goldfisches (*Carassius auratus*). *Zeitschrift für Zellforsch. und Mikroskopische Anat.* 138, 439–454. doi: 10.1007/BF00307104

Brinkmann, A., and Schild, D. (2016). One special glomerulus in the olfactory bulb of *Xenopus laevis* tadpoles integrates a broad range of amino acids and mechanical stimuli. *J. Neurosci.* 36, 10978–10989. doi: 10.1523/JNEUROSCI.4631-15.2016

Byrd, C. A., and Brunjes, P. C. (1995). Organization of the olfactory system in the adult zebrafish: histological, immunohistochemical, and quantitative analysis. *J. Comp. Neurol.* 358, 247–259. doi: 10.1002/cne.903580207

Calvo-Ochoa, E., and Byrd-Jacobs, C. A. (2019). The olfactory system of zebrafish as a model for the study of neurotoxicity and injury: Implications for neuroplasticity and disease. *Int. J. Mol. Sci.* 20:1639. doi: 10.3390/ijms20071639

Carr, V. M., Farbman, A. I., Colletti, L. M., and Morgan, J. I. (1991). Identification of a new non-neuronal cell type in rat olfactory epithelium. *Neuroscience* 45, 433–449. doi: 10.1016/0306-4522(91)90239-K

Chia, J. S. M., Wall, E. S., Wee, C. L., Rowland, T. A. J., Cheng, R.-K., Cheow, K., et al. (2019). Bacteria evoke alarm behaviour in zebrafish. *Nat. Commun.* 10:3831. doi: 10.1038/s41467-019-11608-9

Dando, S. J., Mackay-Sim, A., Norton, R., Currie, B. J., St John, J. A., Ekberg, J. A. K., et al. (2014). Pathogens penetrating the central nervous system: Infection pathways and the cellular and molecular mechanisms of invasion. *Clin. Microbiol. Rev.* 27, 691–726. doi: 10.1128/CMR.00118-13.

Datta, N. C., and Bandopadhyay, S. K. (1997). Ultrastructure of cell types of the olfactory epithelium in a catfish, *Heteropneustes fossilis* (Bloch). *J. Biosci.* 22, 233–245. doi: 10.1007/BF02704736

Demirler, M. C., Sakizli, U., Bali, B., Kocagöz, Y., Eski, S. E., Ergönen, A., et al. (2019). Purinergic signalling selectively modulates maintenance but not repair neurogenesis in the zebrafish olfactory epithelium. *FEBS J.* 287, 2699–2722. doi: 10.1111/febs.15170

DePasquale, J. A. (2020). Tropomyosin and alpha-actinin in teleost rodlet cells. *Acta Zool.* 00, 1–10. doi: 10.1111/azo.12344

Desban, L., Prendergast, A., Roussel, J., Rosello, M., Geny, D., Wyart, C., et al. (2019). Regulation of the apical extension morphogenesis tunes the mechanosensory response of microvilliated neurons. *PLoS Biol.* 17:e3000235. doi: 10.1371/journal.pbio.3000235

Dezfuli, B. S., Capuano, S., Simoni, E., Previati, M., and Giari, L. (2007). Rodlet cells and the sensory systems in zebrafish (*Danio rerio*). *Anat. Rec.* 290, 367–374. doi: 10.1002/ar.20507

Djenoune, L., Khabou, H., Joubert, F., Quan, F. B., Figueiredo, S. N., Bodineau, L., et al. (2014). Investigation of spinal cerebrospinal fluid-contacting neurons expressing PKD2L1: evidence for a conserved system from fish to primates. *Front. Neuroanat.* 8:26. doi: 10.3389/fnana.2014.00026

Dummer, A., Poelma, C., DeRuiter, M. C., Goumans, M.-J. T. H., and Hierck, B. P. (2016). Measuring the primary cilium length: Improved method for unbiased high-throughput analysis. *Cilia* 5:7. doi: 10.1186/s13630-016-0028-2

Dunn, T. W., Mu, Y., Narayan, S., Randlett, O., Naumann, E. A., Yang, C.-T., et al. (2016). Brain-wide mapping of neural activity controlling zebrafish exploratory locomotion. *Elife* 5:e12741. doi: 10.7554/eLife.12741

Dutton, J. R., Antonellis, A., Carney, T. J., Rodrigues, F. S. L. M., Pavan, W. J., Ward, A., et al. (2008). An evolutionarily conserved intronic region controls the spatiotemporal expression of the transcription factor Sox10. *BMC Dev. Biol.* 8:105. doi: 10.1186/1471-213X-8-105

Dutton, K. A., Pauliny, A., Lopes, S. S., Elworthy, S., Carney, T. J., Rauch, J., et al. (2001). Zebrafish colourless encodes *sox10* and specifies non-ectomesenchymal neural crest fates. *Development* 128, 4113–4125.

Elsaesser, R., and Paysan, J. (2007). The sense of smell, its signalling pathways, and the dichotomy of cilia and microvilli in olfactory sensory cells. *BMC Neurosci.* 8:S1. doi: 10.1186/1471-2202-8-S3-S1

Esterberg, R., Hailey, D. W., Coffin, A. B., Raible, D. W., and Rubel, E. W. (2013). Disruption of intracellular calcium regulation is integral to aminoglycoside-induced hair cell death. *J. Neurosci.* 33, 7513–7525. doi: 10.1523/JNEUROSCI.4559-12.2013

Esterberg, R., Linbo, T., Pickett, S. B., Wu, P., Ou, H. C., Rubel, E. W., et al. (2016). Mitochondrial calcium uptake underlies ROS generation during aminoglycoside-induced hair cell death. *J. Clin. Invest.* 126, 3556–3566. doi: 10.1172/JCI84939

Finger, T. E., Böttger, B., Hansen, A., Anderson, K. T., Alimohammadi, H., and Silver, W. L. (2003). Solitary chemoreceptor cells in the nasal cavity serve as sentinels of respiration. *Proc. Natl. Acad. Sci. U. S. A.* 100, 8981–8986. doi: 10.1073/pnas.1531172100

Fujita, T. (1989). Present status of paraneuron concept. *Arch. Histol. Cytol.* 52, 1–8. doi: 10.1679/aohc.52.Suppl_1

Genovese, F., and Tizzano, M. (2018). Microvillous cells in the olfactory epithelium express elements of the solitary chemosensory cell transduction signaling cascade. *PLoS One* 13:e0202754. doi: 10.1371/journal.pone.0202754

Gillespie, P. G., and Müller, U. (2009). Mechanotransduction by hair cells: models, molecules, and mechanisms. *Cell* 139, 33–44. doi: 10.1016/j.cell.2009.09.010

Grosmaitre, X., Santarelli, L. C., Tan, J., Luo, M., and Ma, M. (2007). Dual functions of mammalian olfactory sensory neurons as odor detectors and mechanical sensors. *Nat. Neurosci.* 10, 348–354. doi: 10.1038/nn1856

Gupta, K., Mohanty, S. K., Mittal, A., Kalra, S., Kumar, S., Mishra, T., et al. (2020). The cellular basis of loss of smell in 2019-nCoV-infected individuals. *Brief. Bioinform.* 00, 1–9. doi: 10.1093/bib/bbaa168

Hansen, A. (2007). Olfactory and solitary chemosensory cells: two different chemosensory systems in the nasal cavity of the American alligator, *Alligator mississippiensis*. *BMC Neurosci.* 8:64. doi: 10.1186/1471-2202-8-64

Hansen, A., and Finger, T. E. (2008). Is TrpM5 a reliable marker for chemosensory cells? Multiple types of microvillous cells in the main olfactory epithelium of mice. *BMC Neurosci.* 9:115. doi: 10.1186/1471-2202-9-115

Hansen, A., and Zeiske, E. (1993). Development of the olfactory organ in the zebrafish, *Brachydanio rerio*. *J. Comp. Neurol.* 333, 289–300. doi: 10.1002/cne.903330213

Hansen, A., and Zeiske, E. (1998). The peripheral olfactory organ of the zebrafish, *Danio rerio*: and ultrastructural study. *Chem. Senses* 23, 39–48. doi: 10.1093/chemse/23.1.39

Hansen, A., and Zielinski, B. S. (2005). Diversity in the olfactory epithelium of bony fishes: Development, lamellar arrangement, sensory neuron cell types and transduction components. *J. Neurocytol.* 34, 183–208. doi: 10.1007/s11068-005-8353-1

Hansen, A., Reutter, K., and Zeiske, E. (2002). Taste bud development in the zebrafish, *Danio rerio*. *Dev. Dyn.* 223, 483–496. doi: 10.1002/dvdy.10074

Harris, J. A., Cheng, A. G., Cunningham, L. L., MacDonald, G., Raible, D. W., and Rubel, E. W. (2003). Neomycin-induced hair cell death and rapid regeneration in the lateral line of zebrafish (*Danio rerio*). *JARO* 4, 219–234. doi: 10.1007/s10162-002-3022-x

Heath, J., and Holifield, B. (1991). Actin alone in lamellipodia. *Nature* 352, 107–108. doi: 10.1038/352107a0

Hernádi, L. (1993). Fine structural characterization of the olfactory epithelium and its response to divalent cations Cd^{2+} in the fish *Alburnus alburnus* (Teleostei, Cyprinidae): a scanning and transmission electron microscopic study. *Neurobiology* 1, 11–31. doi: 10.2298/vetgl0302011f

Höfer, D., and Drenckhahn, D. (1999). Localisation of actin, villin, fimbrin, ezrin and ankyrin in rat taste receptor cells. *Histochem. Cell Biol.* 112, 79–86. doi: 10.1007/s004180050394

Howitt, M. R., Lavoie, S., Michaud, M., Blum, A. M., Tran, S. V., Weinstock, J. V., et al. (2016). Tuft cells, taste-chemosensory cells, orchestrate parasite type 2 immunity in the gut. *Science* 351, 1329–1333. doi: 10.1126/science.aaf1648

Ichikawa, M., and Ueda, K. (1977). Fine structure of the olfactory epithelium in the goldfish, *Carassius auratus*. *Cell Tissue Res.* 183, 445–455. doi: 10.1007/bf00225659

Inaba, Y., Chauhan, V., van Loon, A. P., Choudhury, L. S., and Sagasti, A. (2020). Keratins and plakin family cytolinker proteins control the length of epithelial microridge protrusions. *Elife* 9:e58149. doi: 10.7554/eLife.58149

Iwanaga, T., Fujita, T., and Ito, S. (1982). Immunohistochemical staining of enteroendocrine paraneurons with anti-brain tubulin antiserum. *Biomed. Res.* 3, 99–101. doi: 10.2220/biomedres.3.99

Iwata, R., Kiyonari, H., and Imai, T. (2017). Mechanosensory-based phase coding of odor identity in the olfactory bulb. *Neuron* 96, 1139–1152. doi: 10.1016/j.neuron.2017.11.008

Jessen, J. R., Willett, C. E., and Lin, S. (1999). Artificial chromosome transgenesis reveals long-distance negative regulation of *rag1* in zebrafish. *Nat. Genet.* 23, 15–16. doi: 10.1038/12609

Kawakami, K. (2007). *Tol2*: a versatile gene transfer vector in vertebrates. *Genome Biol.* 8:S7. doi: 10.1186/gb-2007-8-s1-s7

Kermen, F., Franco, L. M., Wyatt, C., and Yaksi, E. (2013). Neural circuits mediating olfactory-driven behavior in fish. *Front. Neural. Circuits* 7:62. doi: 10.3389/fncir.2013.00062

Kimmel, C. B., Ballard, W. W., Kimmel, S. R., Ullmann, B., and Schilling, T. F. (1995). Stages of embryonic development of the zebrafish. *Dev. Dyn.* 203, 253–310. doi: 10.1002/aja.1002030302

Kotrschal, K., Krautgartner, W.-D., and Hansen, A. (1997). Ontogeny of the solitary chemosensory cells in the zebrafish, *Danio Rerio*. *Chem. Senses* 22, 111–118. doi: 10.1093/chemse/22.2.111

Kraus, A., Casadei, E., Huertas, M., Ye, C., Bradfute, S., Boudinot, P., et al. (2020). A zebrafish model for COVID-19 recapitulates olfactory and cardiovascular pathophysiologies caused by SARS-CoV-2. *bioRxiv*. doi: 10.1101/2020.11.06.368191.

Krishnan, J., and Rohner, N. (2017). Cavefish and the basis for eye loss. *Philos. Trans. R. Soc. B Biol. Sci.* 372:20150487. doi: 10.1098/rstb.2015.0487

Kwan, K. M., Fujimoto, E., Grabher, C., Mangum, B. D., Hardy, M. E., Campbell, D. S., et al. (2007). The Tol2kit: A multisite gateway-based construction kit for *Tol2* transposon transgenesis constructs. *Dev. Dyn.* 236, 3088–3099. doi: 10.1002/dvdy.21343

Lin, W., Ezekwe, E. A. D. Jr., Zhao, Z., Liman, E. R., and Restrepo, D. (2008). TRPM5-expressing microvillous cells in the main olfactory epithelium. *BMC Neurosci.* 9:114. doi: 10.1186/1471-2202-9-114

Maier, E. C., Saxena, A., Alsina, B., Bronner, M. E., and Whitfield, T. T. (2014). Sensational placodes: Neurogenesis in the otic and olfactory systems. *Dev. Biol.* 389, 50–67. doi: 10.1016/j.ydbio.2014.01.023

Menco, B. P. M., and Jackson, J. E. (1997). Cells resembling hair cells in developing rat olfactory and nasal respiratory epithelia. *Tissue Cell* 29, 707–713. doi: 10.1016/S0040-8166(97)80046-8

Mongera, A., Singh, A. P., Levesque, M. P., Chen, Y. Y., Konstantinidis, P., and Nüsslein-Volhard, C. (2013). Genetic lineage labeling in zebrafish uncovers novel neural crest contributions to the head, including gill pillar cells. *Development* 140, 916–925. doi: 10.1242/dev.091066

Moran, D. T., Rowley, J. C. III., Aiken, G. R., and Jafek, B. W. (1992). Ultrastructural neurobiology of the olfactory mucosa of the brown trout, *Salmo trutta*. *Microsc. Res. Tech.* 23, 28–48. doi: 10.1002/jemt.1070230104

Morrison, C. M., and Odense, P. H. (1978). Distribution and morphology of the rodlet cell in fish. *J. Fish. Board Can.* 35, 101–116. doi: 10.1139/f78-014

Mosimann, C., Puller, A.-C., Lawson, K. L., Tschopp, P., Amsterdam, A., and Zon, L. I. (2013). Site-directed zebrafish transgenesis into single landing sites with the phiC31 integrase system. *Dev. Dyn.* 242, 949–963. doi: 10.1002/dvdy.23989

Muller, J. F., and Marc, R. E. (1984). Three distinct morphological classes of receptors in fish olfactory organs. *J. Comp. Neurol.* 222, 482–495. doi: 10.1002/cne.902220403

Nüsslein-Volhard, C., and Dahm, R. (2002). *Zebrafish: A Practical Approach*. Oxford: Oxford University Press.

Olivares, J., and Schmachtenberg, O. (2019). An update on anatomy and function of the teleost olfactory system. *PeerJ.* 7:e7808. doi: 10.7717/peerj.7808

Parisi, V., Guerrera, M. C., Abbate, F., Garcia-Suarez, O., Viña, E., Vega, J. A., et al. (2014). Immunohistochemical characterization of the crypt neurons in the olfactory epithelium of adult zebrafish. *Ann. Anat.* 196, 178–182. doi: 10.1016/j.aanat.2014.01.004

Pickett, S. B., Thomas, E. D., Sebe, J. Y., Linbo, T., Esterberg, R., Hailey, D. W., et al. (2018). Cumulative mitochondrial activity correlates with ototoxin susceptibility in zebrafish mechanosensory hair cells. *Elife* 7:e38062. doi: 10.7554/eLife.38062

Pinto, C. S., Khandekar, A., Bhavna, R., Kiesel, P., Pigino, G., and Sonawane, M. (2019). Microridges are apical epithelial projections formed of F-actin networks that organize the glycan layer. *Sci. Rep.* 9:12191. doi: 10.1038/s41598-019-48400-0

Ramírez-Weber, F.-A., and Kornberg, T. B. (1999). Cytonemes : cellular processes that project to the principal signaling center in *Drosophila* imaginal discs. *Cell* 97, 599–607. doi: 10.1016/S0092-8674(00)80771-0

Reid, L., Meyrick, B., Antony, V. B., Chang, L. Y., Crapo, J. D., and Reynolds, H. Y. (2005). The mysterious pulmonary brush cell: A cell in search of a function. *Am. J. Respir. Crit. Care Med.* 172, 136–139. doi: 10.1164/rccm.200502-203WS

Reiten, I., Uslu, F. E., Fore, S., Pelgrims, R., Ringers, C., Diaz Verdugo, C., et al. (2017). Motile-cilia-mediated flow improves sensitivity and temporal resolution of olfactory computations. *Curr. Biol.* 27, 166–174. doi: 10.1016/j.cub.2016.11.036

Rhein, L. D., Cagan, R. H., Orkand, P. M., and Dolack, M. K. (1981). Surface specializations of the olfactory epithelium of rainbow trout, *Salmo gairdneri*. *Tissue Cell* 13, 577–587. doi: 10.1016/0040-8166(81)90028-8

Riedl, J., Crevenna, A. H., Kessenbrock, K., Yu, J. H., Neukirchen, D., Bista, M., et al. (2008). Lifeact: a versatile marker to visualise F-actin. *Nat. Methods* 5, 605–607. doi: 10.1038/nmeth.1220.Lifeact

Rodrigues, F. S. L. M., Doughton, G., Yang, B., and Kelsh, R. N. (2012). A novel transgenic line using the Cre-lox system to allow permanent lineage-labeling of the zebrafish neural crest. *Genesis* 50, 750–757. doi: 10.1002/dvg.22033

Sato, Y., Miyasaka, N., and Yoshihara, Y. (2005). Mutually exclusive glomerular innervation by two distinct types of olfactory sensory neurons revealed in transgenic zebrafish. *J. Neurosci.* 25, 4889–4897. doi: 10.1523/JNEUROSCI.0679-05.2005

Saxena, A., Peng, B. N., and Bronner, M. E. (2013). Sox10-dependent neural crest origin of olfactory microvillous neurons in zebrafish. *Elife* 2:e00336. doi: 10.7554/eLife.00336

Schindelin, J., Arganda-Carreras, I., Frise, E., Kaynig, V., Longair, M., Pietzsch, T., et al. (2012). Fiji: An open-source platform for biological-image analysis. *Nat. Methods* 9, 676–682. doi: 10.1038/nmeth.2019

Schmid, B., Schindelin, J., Cardona, A., Longair, M., and Heisenberg, M. (2010). A high-level 3D visualization API for Java and ImageJ. *BMC Bioinform.* 11:274. doi: 10.1186/1471-2105-11-274

Schneider, C., O'Leary, C. E., and Locksley, R. M. (2019). Regulation of immune responses by tuft cells. *Nat. Rev. Immunol.* 19, 584–593. doi: 10.1038/s41577-019-0176-x

Schulte, E. (1972). Untersuchungen an der regio olfactoria des aals, *Anguilla anguilla* L. *Zeitschrift für Zellforsch. und Mikroskopische Anat.* 125, 210–228. doi: 10.1007/BF00306790

Sekerková, G., Zheng, L., Loomis, P. A., Changyaleket, B., Whitlon, D. S., Mugnaini, E., et al. (2004). Espins are multifunctional actin cytoskeletal regulatory proteins in the microvilli of chemosensory and mechanosensory cells. *J. Neurosci.* 24, 5445–5456. doi: 10.1523/JNEUROSCI.1279-04.2004

Sepahi, A., Kraus, A., Casadei, E., Johnston, C. A., Galindo-Villegas, J., Kelly, C., et al. (2019). Olfactory sensory neurons mediate ultrarapid antiviral immune responses in a TrkA-dependent manner. *Proc. Natl. Acad. Sci. U. S. A.* 116, 12428–12436. doi: 10.1073/pnas.1900083116

Sola, C., Giulianini, P. G., and Ferrero, E. A. (1993). Ultrastructural characterization of the olfactory organ in glass eels, *Anguilla anguilla* (Osteichthyes, Anguilliformes). *Ital. J. Zool.* 60, 253–261. doi: 10.1080/11250009309355820

Tang, W., and Bronner, M. E. (2020). Neural crest lineage analysis: from past to future trajectory. *Development* 147:dev193193. doi: 10.1242/dev.193193

Theriot, J. A., and Mitchison, T. J. (1991). Actin microfilament dynamics in locomoting cells. *Nature* 352, 126–131. doi: 10.1038/352126a0

Tilney, L. G., Derosier, D. J., and Mulroy, M. J. (1980). The organization of actin filaments in the stereocilia of cochlear hair cells. *J. Cell Biol.* 86, 244–259. doi: 10.1083/jcb.86.1.244

Tsujikawa, M., and Malicki, J. (2004). Intraflagellar transport genes are essential for differentiation and survival of vertebrate sensory neurons. *Neuron* 42, 703–716. doi: 10.1016/S0896-6273(04)00268-5

Wakisaka, N., Miyasaka, N., Koide, T., Masuda, M., Hiraki-Kajiyama, T., and Yoshihara, Y. (2017). An adenosine receptor for olfaction in fish. *Curr. Biol.* 27, 1437–1447. doi: 10.1016/j.cub.2017.04.014

Waryani, B., Zhao, Y., Zhang, C., Abbasi, A. R., Ferrando, S., Dai, R., et al. (2015). Surface architecture of the olfactory epithelium of two Chinese cave loaches (Cypriniformes: Nemacheilidae: *Oreonectes*). *Ital. J. Zool.* 82, 179–185.

Waryani, B., Zhao, Y., Zhang, C., Dai, R., and Abbasi, A. R. (2013). Anatomical studies of the olfactory epithelium of two cave fishes *Sinocyclocheilus jii* and *S. furcodorsalis* (Cypriniformes: Cyprinidae) from China. *Pak. J. Zool.* 45, 1091–1101. doi: 10.1080/11250003.2015.1018851

Whitlock, K. E. (2015). The loss of scents: Do defects in olfactory sensory neuron development underlie human disease? *Birth Defects Res. Part C Embryo Today Rev.* 105, 114–125. doi: 10.1002/bdrc.21094

Whitlock, K. E., and Westerfield, M. (2000). The olfactory placodes of the zebrafish form by convergence of cellular fields at the edge of the neural plate. *Development* 127, 3645–3653.

Xiao, T., Roeser, T., Staub, W., and Baier, H. (2005). A GFP-based genetic screen reveals mutations that disrupt the architecture of the zebrafish retinotectal projection. *Development* 132, 2955–2967. doi: 10.1242/dev.01861

Yamamoto, M., and Ueda, K. (1978). Comparative morphology of fish olfactory epithelium - IV. *Bull. Jap. Soc. Sci. Fish.* 44, 1207–1212. doi: 10.2331/suisan.44.1207

Zachar, P. C., and Jonz, M. G. (2012). Confocal imaging of Merkel-like basal cells in the taste buds of zebrafish. *Acta Histochem.* 114, 101–115. doi: 10.1016/j.acthis.2011.03.006

Zhang, X.-Y., Huang, Z.-Q., Ning, T., Xiang, X.-H., Li, C.-Q., Chen, S.-Y., et al. (2018). Microscopic and submicroscopic gradient variation of olfactory systems among six *Sinocyclocheilus* species living in different environments. *Zool. Soc. Japan* 35, 411–420. doi: 10.2108/zs170126

Conflict of Interest: The authors declare that the research was conducted in the absence of any commercial or financial relationships that could be construed as a potential conflict of interest.